2018

# Influence of Chitosan-Alginate Scaffold Stiffness on Bone Marrow Stromal Cell Differentiation

Isabel Arias Ponce
*University of Central Florida*

# INFLUENCE OF CHITOSAN-ALGINATE SCAFFOLD STIFFNESS ON BONE MARROW STROMAL CELL DIFFERENTIATION

by

ISABEL ARIAS PONCE
B.S. Illinois Institute of Technology, 2016
A.A. Miami Dade College, 2013

A thesis submitted in partial fulfillment of the requirements
for the degree of Master of Science
in the Department of Materials Science and Engineering
in the College of Engineering and Computer Science
at the University of Central Florida
Orlando, Florida

Spring Term
2018

Major Professor: Stephen J. Florczyk

# ABSTRACT

Tissue grafts are the gold standard for replacing large volume tissue defects. Yet, they present several risks, including infection, low functional outcomes, and reduced graft integrity. Tissue engineering (TE) combines cells and biomaterial scaffolds to foster tissue growth and remodeling. Bone marrow stromal cells (BMSCs) have been shown to respond to the stiffness of their microenvironment, resulting in differentiation into different lineages. 3D porous chitosan-alginate (CA) scaffolds have been previously demonstrated for bone TE with osteoblasts and BMSCs; however, only a single scaffold composition (4 wt%) was studied. Three CA scaffold compositions (2, 4, 6 wt% CA) were produced. Scanning electron microscopy images were obtained to determine average pore sizes for 2, 4, and 6 wt% CA scaffolds, which were 233, 208, and 146 μm. Compression testing was performed on CA scaffolds in dry and wet conditions, where higher concentrations yielded higher stiffnesses ranging from 0.22 to 5.34 kPa and 21.1 to 47.3 Pa, respectively. Fourier transform infrared spectroscopy performed on the CA scaffolds confirmed polyelectrolyte complex formation for all compositions. Human BMSCs from three donors were seeded on CA scaffolds, cultured in growth media for 14 days, then cultured in adipogenic or osteogenic differentiation media for 28 days to promote differentiation. Our hypothesis was that scaffold stiffness would influence BMSC differentiation, with softer scaffolds promoting adipogenesis and stiffer scaffolds promoting osteogenesis. BMSCs formed multicellular spheroids in all CA scaffold concentrations, while the 2 wt% CA scaffolds had smaller spheroids compared to the 4 wt% and 6 wt% CA scaffolds. Osteogenic and adipogenic differentiation were evaluated with Alizarin Red and Oil Red O staining, respectively. While positive staining was observed in all scaffold compositions, more robust differentiation was expected, thereby disproving our

hypothesis. The polysaccharide composition of the CA scaffolds likely contributed to the spheroid formation and limited differentiation.

# ACKNOWLEDGMENTS

I would like to thank my thesis advisor Dr. Stephen Florczyk for his help with the project, funding, and thesis document. Additionally, I would like to thank fellow graduate students in my group, Kailei Xu and Zi Wang, as well as undergraduate students, Bowen Ding, Minh-Chau Le, and Kathryn Ellett, for all of their help. I would also like to thank my thesis committee chairs, Lorraine Leon, Annette Khaled, and Jiyu Fang, for their suggestions to improve the project and thesis document.

# TABLE OF CONTENTS

# LIST OF FIGURES

# LIST OF TABLES

# CHAPTER 1: INTRODUCTION

Large volume tissue defects caused by trauma, congenital defects, or disease present a great challenge for reconstructive surgeons. While traditional tissue grafts such as allografts and autografts present viable alternatives, there are also many drawbacks associated with them. These types of treatments are an insufficient solution due to their high risk of infection, lack of availability, and poor functional outcome. Tissue engineering is an interdisciplinary field that aims to develop solutions that can help enhance, replace, or restore damaged tissues. The main approach of tissue engineering is to combine cells and biomaterials to develop functional tissues that can be implanted at the site of injury in a patient.

A common approach is to use BMSCs (bone marrow stromal cells) and biomaterial scaffolds resulting in increased osteogenesis in model systems in vitro. It has also been shown that BMSCs are responsive to the stiffness of their microenvironment. Therefore, it is of great importance to better understand cell-material interactions, specifically concerning BMSC microenvironment stiffness and lineage differentiation, in order to move the tissue engineering field forward. Chitosan Alginate (CA) scaffolds have been previously demonstrated for bone tissue engineering applications with osteoblasts and BMSCs [1, 2]. Yet, only a single CA composition (4 wt%) has been studied. This thesis examines the effects of CA scaffold stiffness variations (2, 4, 6 wt%) on the differentiation of three BMSC donors. Understanding BMSC donor variation is an important step towards the ultimate goal of TE, which is to develop biomaterials that have specific regenerative effects in a large patient population.

The first chapter includes a literature review that covers essential topics in the field starting with the clinical need, tissue engineering, and biomaterials for tissue engineering, including a

section on CA scaffolds. The second chapter is the methodology section which includes a description of the CA scaffolds synthesis, materials characterization, cell culture, and cellular analysis. The third chapter presents the results from the scaffold characterization and cell culture studies, including SEM, mechanical testing, FTIR, cell proliferation assays, cell proliferation imaging, and differentiation staining. The fourth chapter covers the discussion and conclusions upon which the relationship between CA scaffold stiffness and BMSC differentiation is elucidated. Variations in BMSC donor morphology and differentiation are also discussed.

## CHAPTER 2: LITERATURE REVIEW

### Clinical Need

Surgical reconstruction of tissue defects is one of today's biggest healthcare challenges and expenditures. When tissue defects are large enough that the body can't heal them on its own, tissue grafts are surgically implanted into the defect site. These types of injuries are called "critical-sized defects" and occur when the non-regenerative threshold of bone tissue has been reached [3]. The 2017 U.S. average estimated cost of all organ transplants was $2.26 billion for people under age 65 and $625 million for people over age 65 [2]. Autografts, which are tissue or organ transplants from one part of a person to another location in the same person, are often considered the "gold standard" for replacing diseased or damaged tissues. Yet, they present several risks including donor site morbidity, infection, low functional and cosmetic outcome, and reduced graft integrity [5]. Allografts, which are tissue or organ transplants from another person, remove the complication of donor site morbidity. However, they can occasionally trigger an immunogenic response which requires recipients to be placed on immunosuppressant drugs to prevent rejection [6]. Additionally, allografts are typically frozen, irradiated and/or lyophilized to reduce the likelihood of disease transmission, which can compromise their mechanical integrity and reduce bioactivity. Therefore, while allografts are a viable tissue replacement alternative, they still carry many of the risks associated with autografts. Additionally, both autografts and allografts have a limited supply that can fail to meet the needs of larger defects.

In order to overcome the issues associated with tissue and organ grafts, scientists and engineers are developing innovative biomaterials to repair or replace damaged tissues. The biomaterials field is highly multidisciplinary and it studies materials with a special focus on their interaction with the biological environment for primarily medical purposes, such as therapeutic or

diagnostic applications [7]. The biology of host-material interactions strongly determines the biocompatibility of a material. Biocompatibility is defined as the ability of a biomaterial to generate an appropriate host response within its application, which includes resistance to blood clotting, resistance to bacterial colonization, and regular healing [3, 4]. Besides their enhanced biocompatibility and increased supply, biomaterials can also be designed to fit the specific tissue graft needs of a patient. Therefore, as the rates of chronic disease and the aging population continue to increase, the human impact and commercial market size for the biomaterials field are projected to expand.

## Tissue Engineering

Tissue engineering is a branch of biomedical engineering that focuses on the design and fabrication of biomaterials to repair or replace damaged tissues and organs by developing substitutes or reconstructing them as an alternative to conventional tissue grafts. The tissue engineering field is highly interdisciplinary as it requires the collaboration of materials scientists, cell biologists, chemists, and engineers. The main strategy is to combine cells and biomaterials that are used to grow or foster the remodeling of tissues and organs [9]. As can be observed in Figure 1, cells can be harvested from a patient (1), expanded through cell culture in vitro (2), seeded into a biomaterial (3), cultured for proliferation (4), and finally implanted at the site of injury in a patient (5).

Three-dimensional (3D) biomaterials recreate the extracellular matrix (ECM) environment and provide mechanical support for newly formed tissues [10]. 3D biomaterials can take different forms, such as nanofiber scaffolds, hydrogels, and 3D porous sponges, among others. Scaffolds are porous biomaterials that (i) promote cell-material interactions and ECM deposition, (ii) allow sufficient gas, nutrient, and growth factor transport for cell survival, proliferation, and

differentiation, (iii) degrade at a controlled rate that matches that of native tissue, (iv) cause minimal inflammation or in vivo cytotoxicity [11]. The 3D scaffold also allows for cell migration and proliferation followed by the secretion of native ECM, which can lead to a complete and natural long term tissue replacement [12].

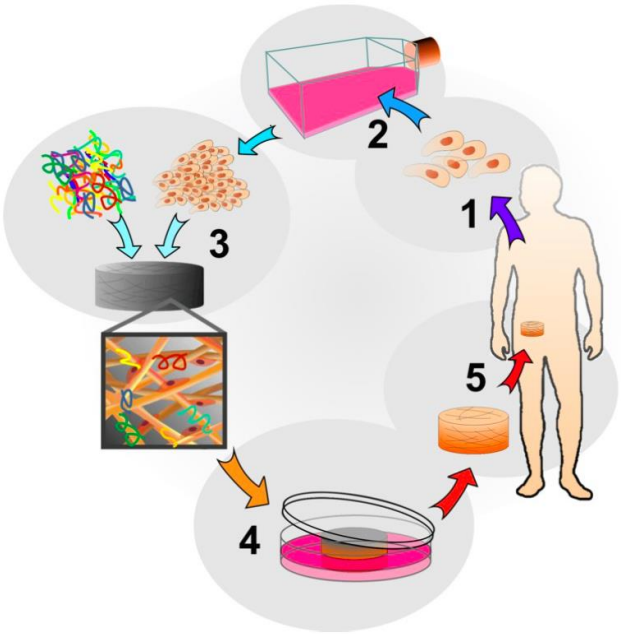


Figure 1. Diagram of the classical tissue engineering model. Cells are harvested from a patient (1), expanded in vitro (2), cultured within a biomaterial scaffold (3-4), and implanted at the site of injury (5).

A common approach in tissue engineering involves harvesting primary stem cells from a patient and culturing them in vitro in a 3D scaffold (Figure 2a). Cultures within scaffolds can be grown in a static (incubator) or a dynamic (bioreactor) environment. After cells proliferate and differentiate into specific tissues, the tissue engineered constructs are implanted at the site of injury to help regenerate damaged tissues. A second approach involves implanting or injecting the 3D scaffolds in vivo and allowing tissue formation and ingrowth to occur in situ (Figure 2b). In this

case, scaffolds are implanted without cells and the patient is used as an incubator to grow the tissue or organ, where cells in the surrounding tissue spontaneously populate the scaffold.

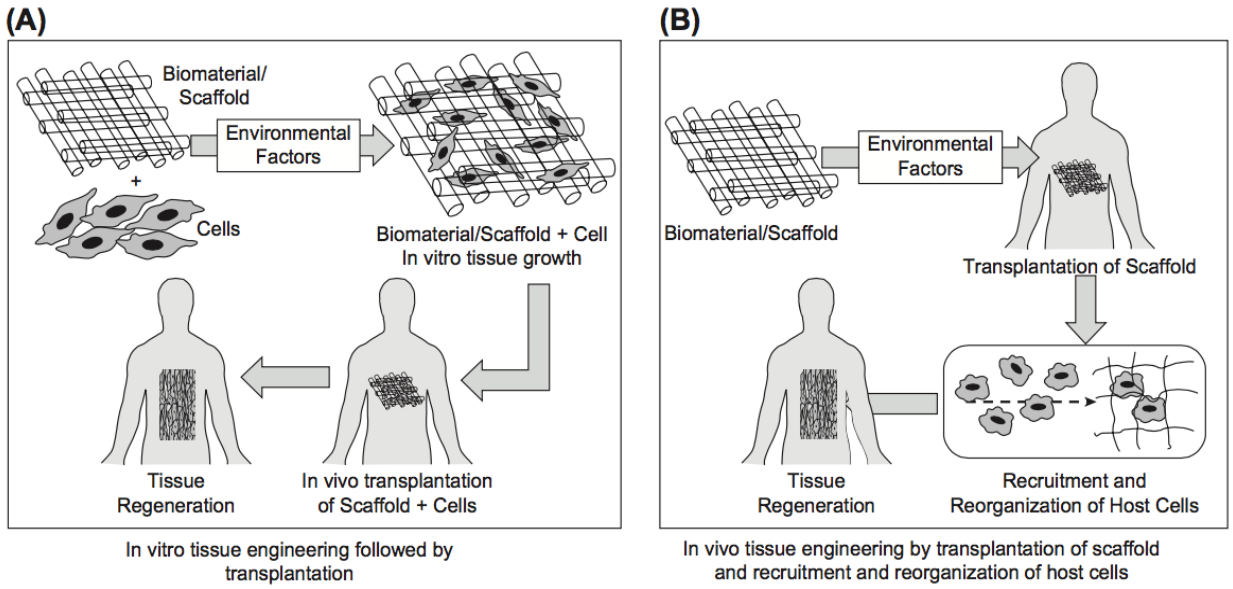


Figure 2. Two main approaches to tissue engineering: (A) Transplantation of in vitro grown tissues and (B) Promotion of tissue regeneration in situ [8].

Biomaterials can be biocompatible, bioactive, and biodegradable depending on their specific application. For example, a hip implant ideally would not be biodegradable in order to provide long term mechanical support, while a skin graft would ideally degrade at a rate matching the regenerating tissue. Biocompatibility prevents an adverse immune response from the patient, bioactivity stimulates cell regeneration, and biodegradation accommodates neo-tissue formation. The scaffold stiffness is typically chosen to match that of the target native tissue and is sufficient to withstand long-term culture and implantation. The main challenges preventing the clinical translation of these products include achieving sufficient biological function from cellularized constructs, optimal host biocompatibility, and cost reduction [13]. It is expected that advances in stem cells, biomaterials, biofabrication, and immunomodulation will speed the clinical application of tissue engineering products by tackling these challenges.

Bone Marrow Stromal Cells in Tissue Engineering

Mesenchymal stem cells (MSCs) are multipotent progenitor cells that have the potential to differentiate into different end-stage mesenchymal cell types, including bone, cartilage, muscle, bone marrow stroma, tendon/ligament, fat, dermis, and other connective tissues, as can be observed in Figure 3 [14]. MSCs reside in a variety of tissues and have the ability to regenerate cell types of the previously mentioned tissues. One type of MSCs, bone marrow stromal cells (BMSCs) are non-hematopoietic adherent cells, a subset of which are skeletal stem cells (SSCs) that can form cartilage, bone, hematopoiesis-supportive stroma, and marrow adipocytes [15]. Besides being undifferentiated, BMSCs have significant self-renewal capacities. Therefore, these cells are very useful in the practices of bone tissue engineering and regenerative medicine.

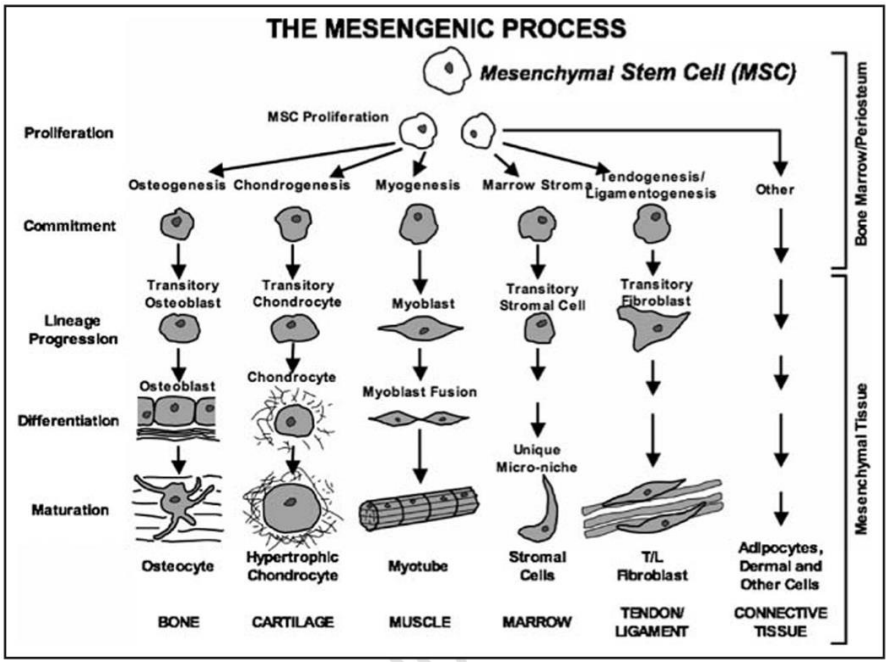


Figure 3. Flowchart of MSC possible commitment, lineage progression, and maturation [16].

One of the most common ways to obtain BMSCs is through bone marrow aspirate from the iliac crest which is considered to be one of its most accessible and enriched sources. Alternatively, adipose derived stromal cells (ADSCs) can be derived from adipose tissue and resemble BMSCs in morphology, phenotype, and differentiation capacity [17]. Both BMSCs and ADCSs have finite life spans despite advancements in long term culture expansion. This occurs since they undergo telomere shortening after each division cycle, which results in gradual senescence [18]. BMSCs were found to decrease in adipogenic potential after 7 passages, with 1 in 2035 cells being capable of differentiating into an adipocyte at passage 7 [19]. BMSCs were found to MSCs play a significant role in development, as well as adult tissue repair.

## BMSCs for Bone Tissue Engineering

The osteogenic induction of BMSCs is a highly programmed process that has been extensively studied in vitro and stimulates osteoblast formation. Osteoblasts are relevant cells for bone tissue engineering since they are in charge of secreting unmineralized, collagen-rich osteoids, upon which bone mineralization occurs [20]. The synthetic glucocorticoid dexamethasone (DEX) stimulates MSC proliferation and osteogenic differentiation [21]. Organic phosphates like β-glycerolphosphate (BGP) enhance osteogenesis by supporting the mineralization and modulation of osteoblast activity [22]. Additionally, free phosphate groups induce the mRNA and protein expression of osteopontin, as well as influence the production and nuclear export of the osteogenic regulatory gene Cbfa1 (core binding factor alpha 1) [28, 29]. Supplements such as L-ascorbic acid (LAA) are also commonly used for osteogenic induction.

The osteogenic differentiation of BMSCs can be confirmed by different bone matrix molecules, mineral crystals, and nodules. An early indicator of BMSC osteogenic differentiation

is the upregulation of alkaline phosphatase activity. Additionally, the presence of mineralized BMSC matrix can be verified with von Kossa or Alizarin Red stains [25]. Osteocalcin, osteopontin, and osteonectin are non-collagenous proteins found in the bone matrix and late osteogenic differentiation markers that can be measured using RT-PCR or proteomically using ELISA [25]. Many natural and synthetic biomaterials have shown promise as carriers for MSC delivery in orthopedic therapeutic applications such as polysaccharides (chitosan, alginate, or hyaluronic acid) PCL, PLA, and PLGA [26]. Advances in the biomaterials field have led to a transition from inert, non-porous materials to highly porous, osteoconductive, cell-matrix composite materials.

## BMSCs for Adipose Tissue Engineering

A large proportion of surgical procedures performed each year are to repair soft tissue defects resulting from a loss of adipose tissue. Therefore, the field of adipose tissue engineering is necessary in these cases. Adipogenic induction of BMSCs is a complex process that is controlled by steroid hormones, transcription factors, and secreted cytokines/adipokines [27]. BMSC adipogenic induction yields adipocytes which are characterized by lipid droplet formation [28]. Bone marrow adipocytes are thought to differentiate from BMSCs in vitro and in vivo. In vitro induction of BMSCs requires specific media supplementations. Adipogenic medium for differentiation usually includes dexamethasone (DEX), 3-isobutyl-1-methylxanthine (IBMX), and indomethacin (IM) [14]. Indomethacin is an anti-inflammatory drug that binds to and activates the transcription factor peroxisome receptor gamma (PPAR-γ).

One of the most important factors in BMSC adipogenic differentiation in PPAR-γ2, which can be detected through RT-PCR [25]. Additionally, Oil Red O is a stain that binds to lipid vacuoles synthesized intracellularly by BMSC-derived adipogenic cells. Common adipogenic

gene products, such as lipoprotein lipase (LPL) and polyclonal antibody anti-P2, can be amplified and detected through RT-PCR [29]. Adipose tissue accumulates lipid vacuoles intracellularly and the extracellular matrix consists of interstitial fibrous tissue, nerve supplies, and vascular lymphatic network [25]. Both synthetic polymers (i.e. PLA, PLGA, PEG) and natural polymers (i.e. collagen, fibrin, gelatin) have been explored for adipose tissue engineering applications with considerable differences in material biocompatibility, mechanical and chemical properties. Collagen is one of the most prevalent natural polymers used for adipose tissue engineering due to its natural prevalence in native adipose ECM, which allows it to promote favorable adipose outcomes [30]. Other natural polymers used in adipose tissue engineering include adipose-derived ECM, decellularized human placenta, hyaluronan, and matrigel.

## Mechanotransduction

Stem cell maintenance and differentiation are influenced by different aspects of their microenvironment, including matrix structure, chemistry, and stiffness. ECM proteins have unique distributions and assembly patterns in different tissues which contribute to developmental processes, since the initiation of matrix expression precedes the generation of pluripotent embryonic stem cells (ESCs) and the onset of cell movement [31]. Additionally, fibronectin regulates cell migration during gastrulation, which occurs as stem cell fate is being established [31]. While ESCs have a temporally changing matrix that may be linked to differentiation, MSCs are known to actively migrate to tissues with different matrix compositions [29]. Therefore, the influence of matrix variations towards MSC differentiation is worth examining.

Cells can actively sense their environment and respond to matrix physical and chemical cues through focal adhesions. Focal adhesions are large protein assembly complexes that

physically couple the ECM to the intracellular actin cytoskeleton [32]. Integrins, the major adhesion receptors, are heterodimers comprised of α and β subunits that have high binding affinity for specific ECM proteins and assemble to link the extracellular and intracellular environments [33]. Additionally, integrins allow for bidirectional outside-in and inside-out force transfer and signal transmission [34]. As cells first secrete matrix proteins in vivo, integrins rearrange these molecules [35]. Adapter proteins, such as talin and viculin, connect integrins to the actin cytoskeleton, which is in turn connected to the nucleus as can be observed in Figure 4 [32]. Therefore, integrins are vital surface transmembrane receptors that can also mediate focal adhesion assembly, cytoskeletal organization, and a cascade of downstream signal transduction events that ultimately regulate gene expression and cell behavior [34].

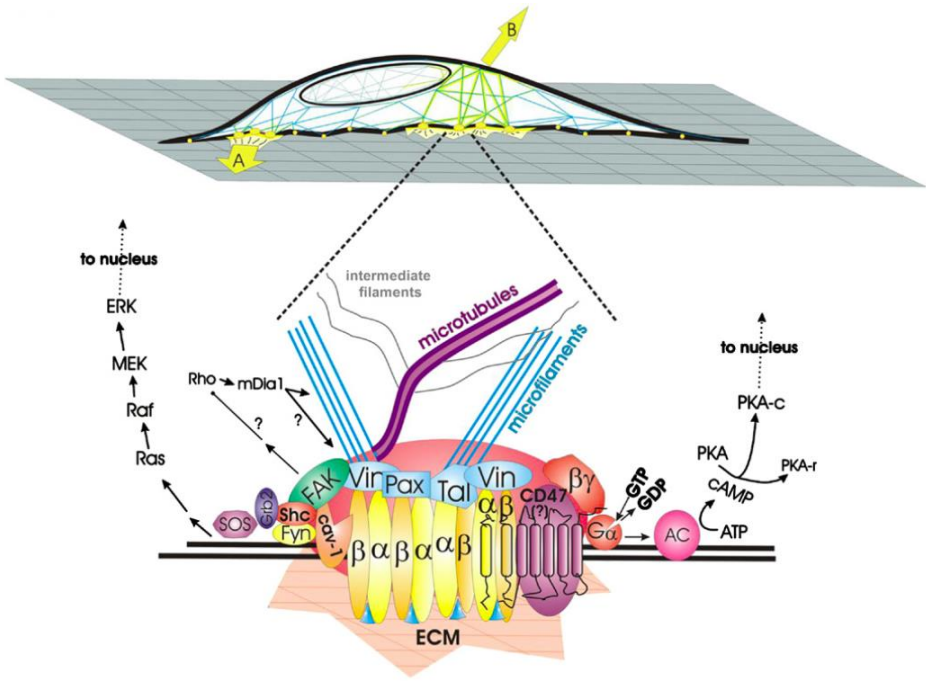


Figure 4. Mechanical forces applied to cells are transmitted across integrin receptors into cytoplasmic domains. Forces concentrated in the focal adhesions stimulate clustering of dimeric (α,β) integrin receptors and of focal adhesion proteins, such as Vinculin (Vin), Paxillin (Pax), and Talin (Tal) [8].

Cells can sense their microenvironment stiffness by pulling against the ECM and assessing its resistance to deformation through focal adhesions. The resistance that a cell feels as it pulls on the ECM is the matrix elastic constant or stiffness, which varies widely across different tissues types. For example, the matrix elastic constant in collagenous bone (100 kPa) is a lot higher than in muscle (10 kPa) and brain (1 kPa) tissues [36]. Cells also alter matrix mechanics by exerting different forces on the ECM, thereby establishing a feedback loop that can influence cell fate and function [32]. This dynamic process of cell-ECM mechanical interactions is called mechanotransduction. These interactions are mediated by integrin proteins within focal adhesion complexes that transmit mechanical forces across the cell surface. Cells exert these cytoskeleton-generated contractile forces through the same integrin-ECM bonds that help them sense matrix stiffness [37]. Focal adhesions are therefore key elements for mechanotransduction, as they bear high mechanical loads and even contain signaling molecules that change their activity under mechanical stress [38]. Forces concentrated within focal adhesions stimulate clustering of dimeric integrin proteins and recruitment of focal adhesion proteins (i.e. talin, vinulin, paxillin) as can be observed in Figure 5 [34].

Biomaterial structure can also strongly influence how a cell senses its microenvironment. For example, when a polymer foam material has pore sizes that are much greater than the cell size, a relatively flat or slightly curved substrate material is effectively presented to the cell as it adheres to a strut. In this case, the basal surface of a cell will attach to the material, which induces a response similar to those observed on planar substrates where high cellular forces occur on stiff materials [32]. On the other hand, smaller pore sizes allow the cell to attach to the material in all dimensions and yield smaller forces than those observed on planar substrates [31]. Yet, it is

important to note that cell-material interactions are fast changing, and that the matrix synthesized by a cell can become a relevant variable to guide cell fate at later timepoints. Besides the stiffness, cells are also exposed to mechanical forces from fluid flow and matrix strain which stimulate differentiation by enhancing cell adhesion, cytoskeleton stiffness, and mechanotransductive signaling.

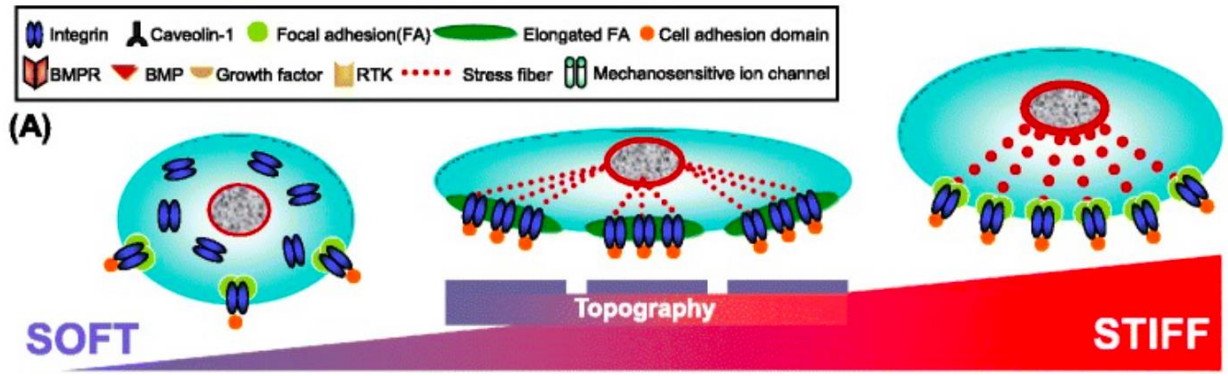


Figure 5. Cells present a small spreading area on soft matrices, associated with poorly defined cytoskeleton, detachment of focal adhesion complexes, and integrin uptake. On substrates with medium stiffness, cells develop elongated focal adhesions and well aligned stress fibers. On rigid matrices, cells display a large spreading area, prominent stress fibers, and enhanced focal adhesion assembly [34].

Cells can also obtain cues regarding matrix chemistry through the specific subset of integrins that interacts with the matrix. Additionally, the presence of certain ECM proteins can influence cell adhesion and differentiation [39]. This occurs through ligand conformational changes that enhance force transmission to integrins on the surface of the cell [40]. Regional differences in receptor-ligand distribution have been shown to control MSC osteogenic differentiation [39]. Matrix chemistry can also be altered by using recombinant proteins that contain adhesion molecules, such as RGD peptides. Even variation in reactive surface groups, such as methyl versus carboxyl, can alter cell adhesion and induce change between self-renewal and

differentiation [41]. Matrix adhesion enhancements, through surface coatings and crosslinking can also improve cell adhesion to matrices and possibly alter integrin expression as well as cell differentiation [42]. Other cell types, besides stem cells, are also responsive to differences in adhesive ligand concentrations, such as malignant phenotypes in mammary epithelial cells that are induced by high levels of fibronectin [43]. Growth factors can also become sequestered within the ECM to be later released by proteolytic degradation or by cell-generated forces [44].

## Biomaterials for Tissue Engineering

A variety of factors influence the material selection for a tissue engineering application, such as biocompatibility, surface chemistry, molecular weight, microstructure, degradability, processability, and mechanical properties [45]. Biomaterials used for tissue repair include metals, ceramics, and polymers. Metal based biomaterials are good for load bearing applications due to their high mechanical properties and resistance to wear and shock. Ceramic based biomaterials are mostly bioinert, have high elastic moduli, and compression resistance. Polymer based scaffolds have unique properties such as high surface to volume ratio, high interconnected porosity, controlled degradation, and tunable mechanical properties [11]. Additionally, polymers and their degradation products usually have lower toxicity and better resemble natural ECM. Therefore, polymer biomaterials have been widely used for the fabrication of medical devices and scaffolds for tissue engineering. Researchers have attempted to grow a variety of tissues on polymer based scaffolds, such as skin [46], bone [47], liver [48], heart grafts [49], pancreas [50], bladder [51], corneas [52], and other soft tissues. Polymer based biomaterials can be natural or synthetic and degradable or non-degradable according to their intended use. The final properties of the polymer scaffold are dependent on its composition, structure, and macromolecular arrangement [11].

## Synthetic Polymers

Synthetic biomaterials are advantageous for tissue engineering applications due to their simple processability into specific shapes and structures, high control of mechanical strength and degradation kinetics, lack of immunogenicity, as well as easy post-modification for specific applications [53]. Additionally, synthetic polymers are usually cheaper than natural materials and can be uniformly fabricated in large quantities with a long shelf time [54]. Generally, synthetic polymers have reproducible and predictable mechanical and physical properties, such as elastic modulus and degradation kinetics, that ease their scale-up and manufacture [11]. While synthetic polymers have great advantages due to the easy tunability of their mechanical properties and degradation kinetics, they also present some drawbacks such as poor biocompatibility, release of acidic degradation products, and rapid loss of mechanical properties [55]. Unfavorable byproducts can obstruct tissue regeneration and even result in inflammation or fibrous encapsulation [55]. Additionally, they lack biological cues which can impede cellular adhesion and interaction [56]. A way to overcome this challenge is to modify synthetic polymers with bioactive molecules.

Some of the most commonly used synthetic polymers in tissue engineering include polyesters such as polylactic acid (PLA), polyglycolic acid (PGA), and their copolymer polylactic-co-glycolic acid (PLGA). These polymers have been widely used for tissue engineering due to their high biodegradability through the hydrolysis of ester bonds, minimal inflammatory response, and highly controlled degradation [57]. PLA has one additional methyl group than PGA in its repeating unit which makes it more hydrophobic and reduces its hydrolysis rate. PLA scaffolds can take months or years to lose their mechanical integrity both in vitro and in vivo [58]. PGA has a relatively hydrophilic nature which causes its rapid degradation in aqueous solutions and in vivo,

ultimately compromising its mechanical integrity within two to four weeks [22]. In order to achieve intermediate degradation rates, PLGA with different lactic to glycolic acid ratios can be synthesized.

## Natural Polymers

Natural polymers were the first materials to have been used medically, since ancient Egyptians used animal tendons as sutures [59]. Due to their bioactive nature, natural polymers have often superior cell-material interactions which enhance their performance within a biological system [11]. Additionally, they are biodegradable, biocompatible, and similar to the ECM. Their main drawbacks include batch to batch variability, lower control of mechanical properties, and limited processability. The two main classes of natural polymers used for tissue engineering applications are proteins and polysaccharides.

Proteins include silk, collagen, fibrin, gelatin, elastin, and keratin, among others. The main motivation for using protein based polymers is that they mimic proteins in the ECM, thereby having the ability to direct cell migration, growth and organization during tissue regeneration. Collagen has 28 different identified types, but type I is the most common in the human body. Collagen is also a major component of the fibrillar extracellular matrix and it provides essential signals for cell regulation, anchorage, migration and proliferation [60]. As a result it has been studied for artificial skin (collagen IV), bone (collagen I), and cartilage (collagen II), resulting in many tissue engineering products [61].

Gelatin is a natural polymer derived from collagen that is known for its biodegradability and biocompatibility within the physiological environment. More specifically, gelatin is obtained by acid and alkaline processing of collagen. Additionally, gelatin is a good carrier of bioactive

molecules, such as fibroblast growth factor, and has low immunogenicity [62], [63]. Gelatin has been widely used for tissue engineering applications, such as in chitosan-gelatin/nanohydroxyapatite composite scaffolds for bone tissue engineering [64]. Silk is a protein polymer that is spun into fibers by lepidoptera larvae, such as silkworms, spiders, etc. Silk has received great attention due to its high strength to weight ratio and slow degradation [65]. Silk fibroin, a natural polymer made by silkworms that can be mass produced, is commonly used as a textile fiber and for surgical sutures in the medical field [66]. Additionally, silk fibroin has been successfully investigated for the tissue engineering of bone, cartilage, and ligaments [67].

Fibrin is a matrix protein made from the fibrinogen precursor, which self-polymerizes in presence of the enzyme thrombin that triggers a coagulation cascade is response to vascular injury [66]. This coagulation response also helps establish a fibrin based provisional matrix at the injury site that provides structural and biochemical support for wound healing. Due to its ability to enhance cell migration, fibrin has been explored for tissue engineering applications [68]. As a result, fibrin has been used to study bone, cartilage, skin, nerve, and spinal cord regeneration [69].

Polysaccharides are macromolecules that consist of monosaccharides linked by o-glycosidic bonds that form branched and linear structures [54]. Polysaccharides include chitosan, alginate, amylose, cellulose, hyaluronic acid, and chondroitin sulfate. Glycosaminoglycans, such as hyaluronic acid and chondroitin sulfate, are polysaccharides naturally found in the ECM that also have excellent biocompatibility and bioactivity [11]. Using polysaccharides for tissue engineering is highly advantageous since they are naturally found in the ECM and contribute to cell signaling and growth [70]. Therefore, polysaccharides are easily recognized in the biological environment and have both high biocompatibility and bioactivity which makes them promising

materials for the tissue engineering field.

Chitosan is a cationic polymer derived from chitin found in the shell of crustaceans that has shown high biocompatibility, ease of scaffold fabrication, and promise for tissue engineering applications in skin, bone, cartilage, and vascular graft regeneration [66]. Chitosan is composed of N-acetyl-glucosamine and N-glucosamine units and it is obtained through the alkaline deacetylation of chitin, a linear polymer made of N-acetyl-glucosamine. Once the degree of deacetylation (DD) of chitin exceeds 50%, the polymer is called chitosan. Chitosan is soluble in dilute acidic conditions, such as in acetic acid solutions, under which its amino groups protonate [71]. Chitosan can be ionically crosslinked, form polyelectrolyte complexes (PEC), or be covalently crosslinked, which allow for pH neutralization and enhanced mechanical properties. PECs form once the cationic chitosan is combined with a negatively charged polymer, such as alginate, to form an ionic network [72]. Chitosan is a biodegradable material as it can be degraded by human enzymes, such as lysozyme. Chitosan has multiple hydroxyl and amino function groups that provide sites for chemical modifications. Therefore, many research groups have explored attaching biomolecules to chitosan by covalent bonding, ionic bonding, or adsorption.

Alginate is brown algae derived anionic polysaccharide that has been used in the form of hydrogels, beads, and scaffolds for tissue engineering applications due to its pro-angiogenic and regenerative properties [73]. The molecular weight of alginate can range from 50 kDa to 100,000 kDa. Alginates are composed of (1,4)-linked β-D-mannuronic acid (M) and α-L-guluronic acid (G) units within homopolymer blocks of similar (i.e. MMMM, GGGG) or alternating sections (i.e. MGMG) [73]. The amounts of similar or alternating blocks is dependent upon the source of the alginate. G blocks are typically stiffer than M blocks due to intramolecular bonding between the

carboxyl and hydroxyl groups, therefore alternating these blocks increases the alginate solubility. A common crosslinking technique for alginate, called ionic crosslinking, involves using divalent cations ($Ca^{2+}$ or $Ba^{2+}$) to form bonds between carboxylic groups of neighboring G units.

Alginate stiffness changes with respect to composition following the trends: MG < MM < GG, while elasticity increases with GG < MM < MG. Therefore, alginate properties can be tuned by changing the M:G ratio, crosslinking method, and molecular weight [37]. While alginate is a natural polymer, it is foreign to mammalian cells and cannot be broken down by enzymes in vivo. In the case of ionically crosslinked alginate, degradation can occur by the release of crosslinking divalent ions into the surrounding medium for monovalent ions. As calcium ions are released, carboxyl anion repulsion further accelerates the swelling and erosion of the alginate chains [74]. Therefore, in vivo control of alginate degradation is poor. Additionally, mammalian cells do not naturally adhere to alginate and this material is relatively biologically inert. In order to improve cell adhesion, ECM proteins and peptides (such as collagen and RGD peptides) can be physically or chemically attached to alginate [28, 29].

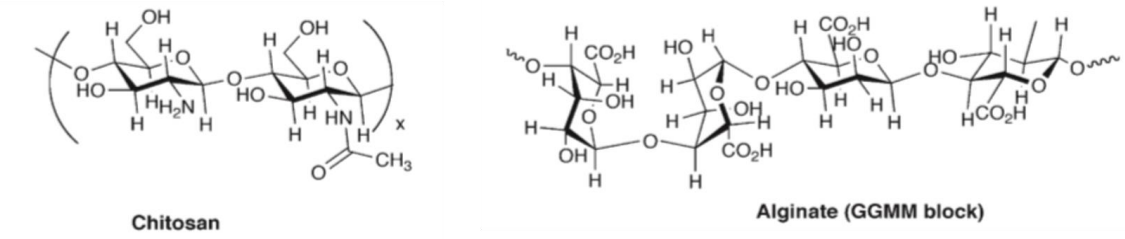


Figure 6.Various natural polymers used for tissue engineering applications [8].

Both chitosan and alginate are polymers that readily absorb excess fluid from their environment. Therefore, scaffolds made of either material can be more prone to degradation within

the physiological environment through bulk erosion. Forming PECs of chitosan and alginate allows for superior mechanical properties due to a lower degree of swelling. While chitosan was effectively degraded by lysozymes, the effect of these enzymes on the degradation of CA complexes was negligible due to strong interactions between the chitosan and alginate polymeric chains for almost 2.5 hours [77]. The stability of chitosan alginate PECs are influenced by charge ratio, molecular weight, ionic strength, pH, and mixing order [78]. Since polymer ratios can change the rate of biodegradation, chitosan alginate polymer blends have high potential for tissue engineering applications.

## Chitosan-Alginate Materials

Polysaccharide biomaterials are of high relevance to the tissue engineering field since they are naturally derived and have a chemical structure that closely mimics that of glycosaminoglycans in native ECM. When cationic chitosan and anionic alginate are blended together in solution, they can form PECs due to electrostatic interactions. Chitosan-Alginate (CA) PEC formation is dependent on solution pH, polymer molecular weight, and alginate to chitosan ratio. While alginate is naturally non-adhesive to mammalian cells, CA materials exhibit better cell adhesion due to the ability of positively charged chitosan to adsorb serum proteins. Therefore, CA materials combine the advantages of its independent polymer components while reducing the drawbacks.

CA materials can be processed to induce a phase separation that gives a porous microstructure to ensure cell attachment, tissue growth, and allow the flow of nutrients. This can be accomplished by freeze casting and freeze drying CA solutions. Scaffold porosity is dependent on many processing parameters, including freezing temperature, molecular weight of polymer, and polymer solution concentrations. Solution viscosity, which is dependent on concentration, has

been found to be the main parameter regulating pore structure and scaffold mechanical properties [79]. These parameters influence the shape and size of ice crystals that form scaffold pores after freeze drying. CA scaffolds have been previously fabricated to yield pore sizes from 100 to 300 μm [1]. Additionally, CA scaffolds have been demonstrated to have superior mechanical properties than chitosan scaffolds due to strong ionic interactions between chitosan and alginate to form PECs.

CA biomaterials investigated for tissue engineering applications with in vitro studies have been shown to promote cell adhesion and proliferation for cartilage, bone, and embryonic stem cell (ESC) cultures [79]. CA scaffolds demonstrated for bone tissue engineering with osteoblasts showed that cells attached to the scaffold, proliferated, and deposited calcified matrix. Also, calcium deposits on CA scaffolds were observed starting the fourth week after implantation [1]. CA scaffolds were also investigated for cartilage tissue engineering with HTB-94 cells, where cell proliferation was found to be faster in CA scaffolds than in pure chitosan scaffolds. Additionally, HTB-94 cells remained spherical in the CA scaffolds while showing an elongated morphology in the chitosan scaffolds [80]. CA scaffolds have also been investigated for culturing human embryonic stem cells (hESCS) and were demonstrated to support cell renewal without conditioned medium or feeder cell support [81].

In addition to in vitro cell culture studies, CA scaffolds have been demonstrated to support functional bone tissue engineering in vivo with a critical size calvarial defect model. CA scaffolds were found to support undifferentiated MSCs in culture for 14 days in vitro with a spherical morphology. In vivo tests showed that the best defect closure was obtained for CA scaffolds with bone morphogenetic protein-2 (BMP-2) treatment [2].

Previous studies with CA scaffolds have demonstrated support of stem cell self-renewal while maintaining stem cells undifferentiated but only one CA scaffold composition (4 wt% CA) was investigated. By varying the CA scaffold concentration (2-6 wt% CA), we can evaluate if substrate stiffness guides BMSC differentiation into either adipogenic or osteogenic lineages. Therefore, this study will examine cell-material interactions in CA scaffolds and determine if mechanotransductive signaling from varying substrate stiffness can overcome BMSC stemness to support differentiation.

# CHAPTER 3: METHODOLOGY

## Materials

Chitosan (practical grade, >75% deacetylated, MW=190,000 - 375,000 Da), alginate (from brown algae), dexamethasone (DEX), isobutylmethylxanthine (IBMX), indomethacin (IM), β-glycerolphosphate (BGP), L-ascorbic acid 2-phosphate (LAA) were purchased from Sigma-Aldrich (St. Louis, MO). Alpha minimum essential medium (α-MEM), penicillin/streptomycin (P/S), L-glutamine (L-glut), Dulbecco's phosphate buffered saline (D-PBS), trypsin-EDTA (0.25%), Alamar Blue solution, CellTracker chloromethyl-benzamidodialkylcarbocyanine (CM-DiI) and Hoescht 33342 stains were purchased from Fisher Scientific (Waltham, MA). Fetal bovine serum (FBS) was purchased from Atlanta Biologicals (Atlanta, GA). Accumax was purchased from Innovative Cell Technologies (San Diego, CA). BMSCs from seven donors were purchased from RoosterBio (Frederick, MD). Additional information regarding BMSC donor gender and age can be found in Table 1.

Table 1. BMSC donor information.

| Donor | Sex | Age |
|---|---|---|
| 12 | M | 33 |
| 16 | F | 29 |
| 37 | M | 43 |
| 49 | M | 23 |
| 55 | M | 22 |
| 70 | F | 20 |
| 81 | M | 25 |

## CA scaffold synthesis

2, 4, and 6 wt% CA scaffolds were prepared according to previously published methods [1, 2]. The chitosan and alginate solutions were prepared separately and equal amounts of chitosan and alginate were used to prepare the CA solutions. To synthesize a 4 wt% CA scaffold, 4 wt% chitosan and 4 wt% alginate solutions were prepared. A 4 wt% chitosan solution was prepared in 1 wt% acetic acid and a 4 wt% alginate solution was prepared in DI water. Both solutions were prepared by dissolving the raw material powders in their respective solvents and mixing three times with a Thinky mixer (Thinky Corporation, Laguna Hills, CA) at 2000 rpm for several minutes. Excess heat in the mixer was dissipated between samples to keep mixing temperatures consistent in all solutions. Both solutions were aged overnight and mixed several times in a Thinky mixer. The 4 wt% chitosan solution with higher viscosity was added to the 4 wt% alginate solution with lower viscosity and the combined 4 wt% CA solution was mixed several times with a Thinky mixer at 2000 rpm. This step helps the formation of CA PECs. After mixing the solutions, the 4 wt% CA solution was casted in 12-well plates and its pH was measured. CA samples were refrigerated at 4°C for 1 hour, frozen at -20 °C overnight, and lyophilized for 2 days. CA scaffolds were then sectioned at 2 mm thickness, crosslinked in 0.2 M $CaCl_2$ for 15 minutes under vacuum, and washed three times with DI water. Sterilization was performed by soaking scaffolds in 70% ethanol solution for 30 minutes under vacuum, washing three times with D-PBS, and washing overnight with D-PBS in the shaker plate. The CA method was adapted to produce different scaffold properties by varying the polymer and acetic acid concentrations to yield 2, 4, and 6 wt% CA scaffolds as can be observed in Tables 2 and 3.

Table 2. 2, 4, and 6 wt% Alginate concentrations in DI water.

| Wt% | Alginate (g) | DI water (g) |
|---|---|---|
| **2** | 2.084 | 100 |
| **4** | 4.167 | 100 |
| **6** | 6.25 | 100 |

Table 3. 2, 4, and 6 wt% Chitosan concentrations in acetic acid solutions.

| Wt% | Chitosan (g) | Acetic acid (g) | DI water (g) |
|---|---|---|---|
| **2** | 2.084 | 0.5 | 99.5 |
| **4** | 4.167 | 1.0 | 99.0 |
| **6** | 6.25 | 1.5 | 98.5 |

## Scanning Electron Microscopy

CA scaffold microstructure was analyzed with scanning electron microscopy (SEM). Samples were sputter coated with palladium-gold (Pd-Au) before being imaged with a JSM 6480 (JEOL, Tokyo, Japan). Average pore sizes were determined by drawing five equally spaced line segments on the SEM micrographs at 50× magnification, counting the number of pores intersecting each line, and finding the ratio of intercepts to line length. This method was adapted from the ASTM E112-13 standard method for determining average grain size [82].

## Mechanical Testing

The stiffness of the scaffolds were assessed in both wet and dry conditions at room temperature using the AGS-X mechanical tester (Shimadzu, Japan). The CA scaffolds were cut into 10 mm x 10 mm x 10 mm cubes and compressed at a rate of 0.4 mm/min using a 500 N load cell until reaching 40% of the initial height. Scaffolds were crosslinked with 0.2 M $CaCl_2$, washed with D-PBS, and stored in D-PBS prior to mechanical compression testing for wet conditions. Young's moduli were calculated from the slopes of the linear regions of the stress–strain curves.

## Fourier Transform Infrared Spectroscopy

PEC formation was assessed in the CA scaffold array with Fourier Transform Infrared (FTIR) Spectroscopy. Freeze dried scaffolds were ground with potassium bromide into a fine powder. The mixed powder was compressed to a transparent pellet of 0.8-1 mm thickness with the Quick Press KBr Pellet Kit (International Crystal Lab, Garfield, NJ). Scaffolds were analyzed with FTIR (Nexus 870, Thermo Scientific, Waltham, MA) with 300 scans at 8 $cm^{-1}$ resolution.

## Cell culture

BMSCs were expanded for six days in T-150 flasks (Corning, Waltham, MA). Cultures were maintained in fully supplemented α-MEM with 16.5% FBS, 1% P/S, and 1% L-glut at 37 °C and 5% $CO_2$ in a fully humidified incubator. BMSCs were detached with 0.25% Trypsin-EDTA. Prior to seeding, cell pellets were resuspended in D-PBS at $1\times10^6$ cell/mL. Then, cell solutions were stained with CellTracker CM-DiI stain (5 μL/mL), incubated at 37 °C for 5 minutes, 4 °C for 15 minutes, and washed three times with D-PBS. Afterwards, cell solutions were stained with Hoescht 33342 stain (1 μL/mL), incubated at room temperature for 20 minutes, and washed three times with D-PBS. Cells were resuspended in media at $2\times10^6$ cell/mL concentration and seeded

dropwise onto damp CA scaffolds in 12-well plates at 200,000 cells per scaffold with 100 μL of cell suspension. Scaffolds were incubated for 2 hours after cell seeding before 1.5 mL of cell media were added to the wells. For 2D samples, 500 μL of cell solution (100,000 cells) and 1 mL of cell media were added to the 12-well plate wells. Media was replaced at least every 2 days. The cultures were allowed to proliferate for 14 days, then the cultures were switched to adipogenic or osteogenic media and cultured for an additional 28 days to induce differentiation. Adipogenic media contained 0.5 μM DEX, 0.5 μM IBMX, and 50 μM IM in fully supplemented α-MEM. Osteogenic media contained 10 nM DEX, 20 mM BGP, and 50 μM LAA in fully supplemented α-MEM.

Cell proliferation analysis

The Alamar Blue assay was used to assess cell proliferation in CA scaffolds and 2D wells at 2, 7, and 14 day timepoints following the manufacturer's protocols. 1.5 mL of Alamar Blue solution (10 v/v% in media) was added to each sample well and incubated for 2.5 hours. Afterwards, the Alamar Blue solutions were transferred to a black-bottom 96-well plate and was read with fluorescence at 560 nm excitation, 590 nm emission with a Cytation5 imaging multi-mode reader (Biotek, Winooski, VT). Samples were washed once with D-PBS and 1.5 mL of cell culture medium was added. Cell numbers were calculated from standard curves with known cell numbers for each cell donor.

Cell imaging

Live cell fluorescence imaging was performed to observe cell morphology and nuclei with CM-DiI and Hoescht 33342 stains at the 3, 7, and 14 day time points. Samples were imaged with the Cytation5 cell imaging multi-mode reader (Biotek, Winooski, VT) at 4× and 20×

magnifications with DAPI and RFP filters. Brightfield images were also obtained for all samples at both magnifications.

Alizarin Red and Oil Red O staining

Scaffolds and 2D samples were fixed with 3.7% formaldehyde solution for 1 hour and washed three times with D-PBS prior to staining. Samples treated with adipogenic differentiation media were immersed with 60% isopropanol for 10 minutes, stained with Oil Red O staining solution for 15 minutes, and washed three times with D-PBS. Samples treated with osteogenic differentiation media were processed to prepare slides for histology analysis using the Leica ASP 300S tissue processor, Leica EG1150 C tissue embedder, and Leica RM 2235 microtome (Wetzlar, Germany). Histology samples were cut into 16 µm sections, mounted on slides, dewaxed, rehydrated, stained with Alizarin Red staining solution for 10 minutes, and washed three times with DI water. All samples were imaged using the Cytation5 imaging multi-mode reader.

# CHAPTER 4: RESULTS AND DISCUSSION

## Scanning Electron Microscopy

Scaffolds of 2, 4, and 6 wt% CA concentrations were produced successfully and were stable in aqueous conditions after crosslinking. SEM images of all CA scaffold compositions (2, 4, 6 wt%) were obtained at two different magnifications (50, 200×) in order to better assess the pore structure changes resulting from variations in composition. CA scaffolds yielded an interconnected porous structure as a result of the sublimation of ice from CA solutions during lyophilization. Higher CA scaffold concentrations (4, 6 wt%) have smaller pore structures than lower CA scaffold concentrations (2 wt%), as can be observed in Figure 7.

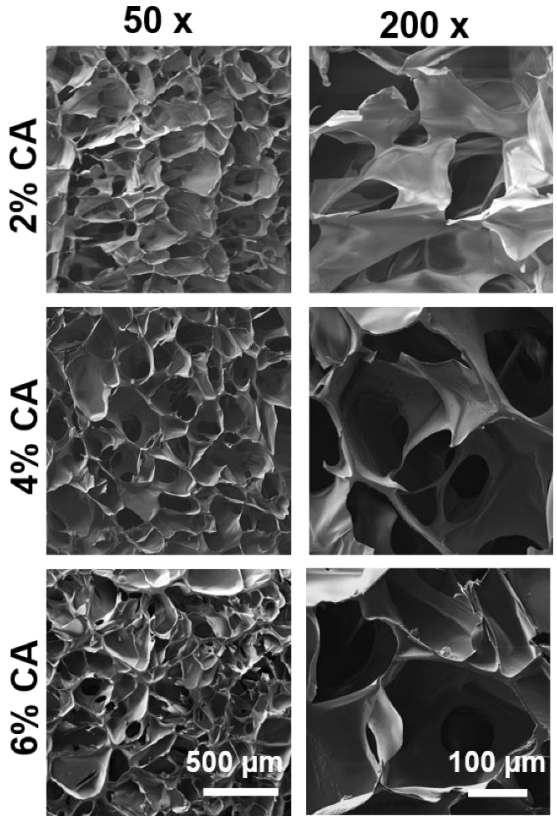


Figure 7. SEM images of 2, 4, 6 wt% CA scaffolds taken at 50 and 200× magnifications.

Porosity variations among the CA scaffold array compositions were also quantitatively assessed by calculating the average pore sizes for all CA scaffold compositions. Our approach was adapted from the ASTM E112-13 standard method for determining average grain sizes [82]. The average pore size values for 2, 4, and 6 wt% CA scaffolds can be found in Table 4. As expected, average pore sizes decrease with increasing CA scaffold concentrations. This occurs as increasing CA concentrations with higher polymer densities reduce the size of ice crystals formed, thereby giving an overall smaller microporous structure.

Table 4. CA scaffold average pore sizes.

| Scaffolds | Average Pore Size (μm) | Standard Deviation |
|---|---|---|
| 2% CA | 233.3 | 23.7 |
| 4% CA | 208.2 | 37.9 |
| 6% CA | 146 | 17.8 |

## Mechanical Testing

The elastic modulus of all CA scaffold compositions (2, 4, 6 wt%) was determined with compression mechanical testing (Figure 8). Besides measuring the elastic modulus of the CA scaffolds after lyophilization (dry condition), the elastic modulus of CA scaffolds was also tested under wet conditions. Samples prepared for the wet condition were crosslinked, sterilized, and washed overnight prior to compression testing. The elastic modulus of CA scaffolds in the wet condition was relevant since it better resembled the mechanical properties BMSCs are exposed to during in vitro cultures.

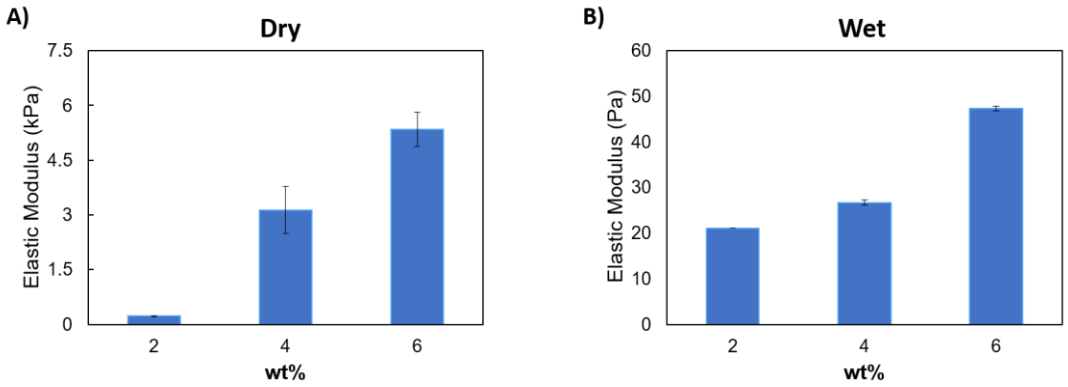

Figure 8. CA scaffold compression mechanical testing under dry (A) and wet (B) conditions.

The mechanical properties of CA scaffolds in dry conditions were one to two orders of magnitudes higher than CA scaffolds in wet conditions. This decrease in Young's modulus has also been observed in wet conditions compared to dry conditions by other research groups in a variety of polymer substrates [83]. This type of behavior is mainly due to the plasticizing effect of water in the CA scaffolds, which allows CA polymer chain fibers a greater freedom of motion. Due to higher porosity size at the lower CA scaffold concentrations, this plasticizing effect yields a lower elastic modulus for 2 wt% CA scaffolds than 4 and 6 wt% CA scaffolds.

Measuring the differences in CA scaffold stiffness under wet conditions (that mimic in vitro conditions) is key to understanding BMSC behavior, since BMSCs grow in the wet environment during cell culture. Moreover, it has been demonstrated that BMSCs commit to specific lineages with high sensitivity to matrix stiffness [75]. Substrate elasticity also affects other important cellular processes such as cell adhesion, growth, proliferation, and differentiation [84].

CA scaffold elasticity values in the dry condition (0.22–5.34 kPa) best match the elastic modulus for brain tissue (0.1–1 kPa) with the 2 wt% CA scaffold stiffness (0.22 kPa). On the other hand, 4 and 6 wt% CA scaffolds in the dry condition (3.14 and 5.34 kPa) have stiffnesses values between the upper limit for brain and lower limit for muscle tissue (1–8 kPa). CA scaffold elasticity values in the wet condition (21.1–47.3 Pa) are lower than typical brain tissue stiffness

measurements. While previous studies have demonstrated 2D materials with similar stiffnesses to native tissue for BMSC differentiation into multiple lineages, the effects of 3D porous microenvironment stiffness variations on BMSC cell fate have not been established. Therefore, this study will help elucidate the relationship of CA scaffolds stiffness and BMSC differentiation.

## Fourier Transform Infrared Spectroscopy

FTIR was performed for all CA scaffold compositions and in chitosan and alginate only scaffolds in order to confirm PEC formation (Figure 9). The characteristic peak in alginate for the carboxylic acid group can be observed at 1600 $cm^{-1}$. The characteristic peaks in chitosan for the amide group and primary amine N-H bending were observed at 1650 and 1590 $cm^{-1}$ respectively. The CA scaffold PEC formation was demonstrated by the merging of the characteristic peaks for chitosan and alginate to form a broader peak at 1630 $cm^{-1}$. The characteristic peak at 1630 $cm^{-1}$ was observed in the 2, 4, and 6 wt% CA scaffolds, indicating PEC formation at all concentrations.

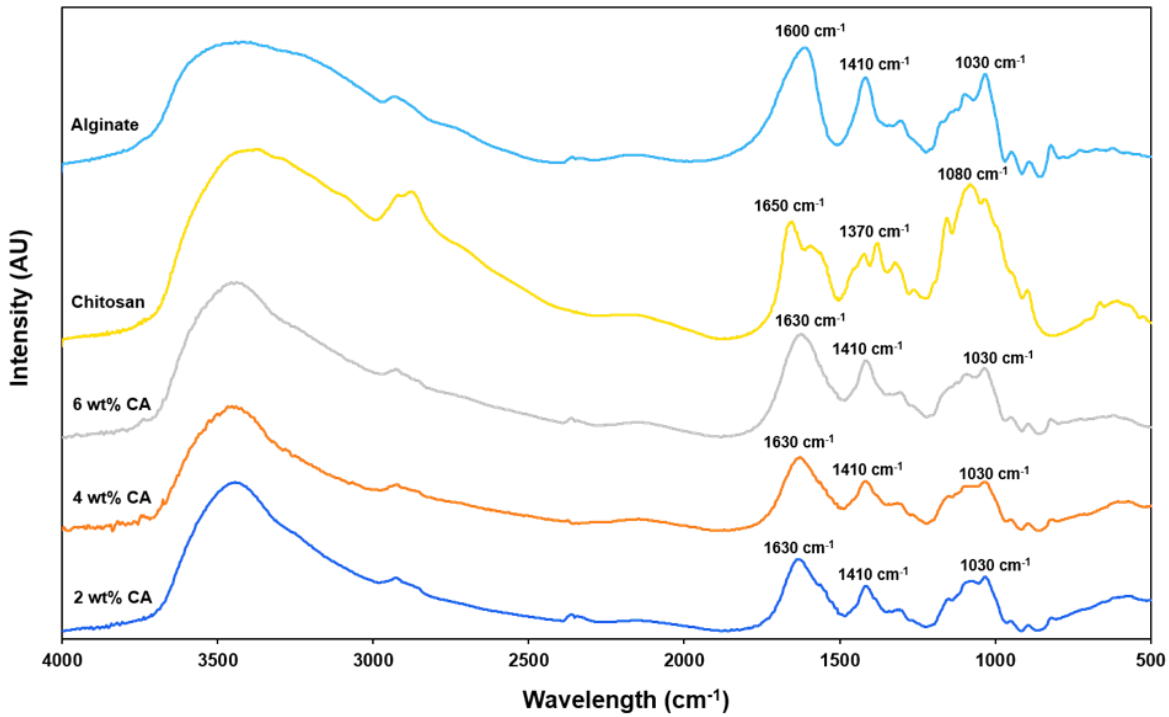


Figure 9. FTIR spectra of 2, 4, 6 wt% CA, chitosan, and alginate scaffolds.

Preliminary Study: Evaluation of Proliferation for Multiple BMSC Donors

Prior to starting the BMSC differentiation study, a preliminary trial testing the proliferation of 7 BMSC donors within the 4 wt% CA scaffold composition was carried out by using the Alamar Blue proliferation assay. All BMSC donors increased in cell number with increasing timepoints and BMSC donor 81 reached the highest cell number in the 4 wt% CA scaffold, as can be observed in Figure 10.

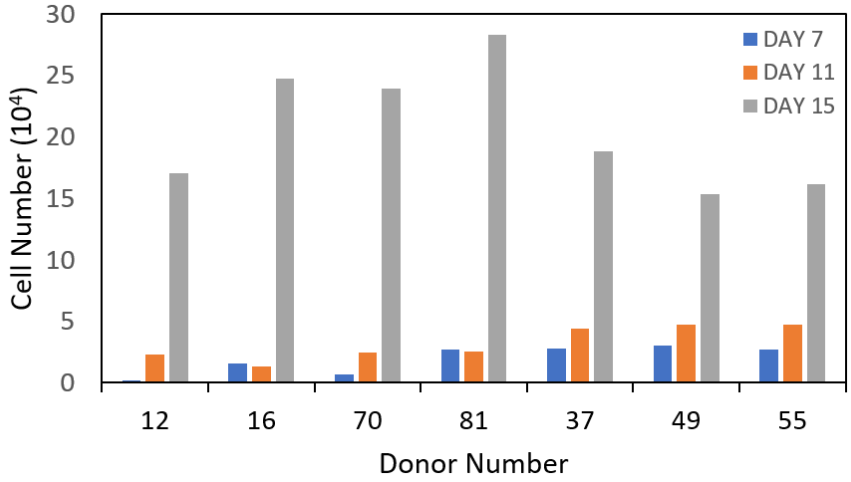


Figure 10. BMSC Multiple Donor proliferation study in 4 wt% CA scaffolds.

Additionally, all BMSC donors formed cell spheroids in the 4 wt% CA scaffolds as can be observed in Figure 11. Spheroid formation could be attributed to the fact that CA scaffolds are polysaccharide-based and lack matrix proteins to facilitate cell adhesion and cell spreading. Donors 12, 37, and 81 formed cell spheroids of similar size.

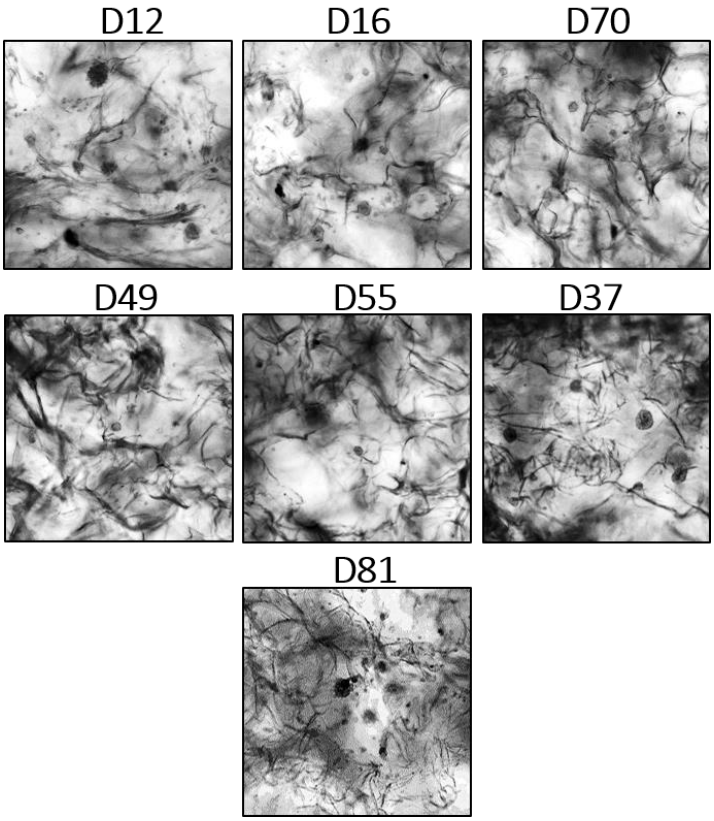


Figure 11. BMSC donors cluster into cell spheroids in 4 wt% CA scaffolds at day 7 of proliferation.

Spheroid size also varied with time for all CA scaffold compositions, with the greatest size of spheroids being observed at day 3 and decreasing afterwards, as can be observed in Figure 12. It is possible that at later timepoints, BMSCs begin to migrate within the scaffolds, thereby decreasing spheroid size.

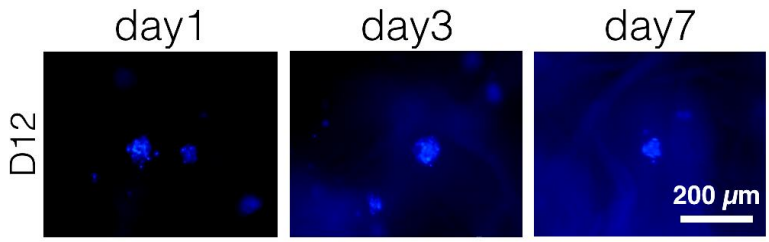

Figure 12. BMSC donor 12 in 4 wt% CA scaffolds at days 1, 3, and 7. Cell nuclei were observed with the Hoescht live fluorescent stain.

This preliminary study helped us evaluate the proliferation of the BMSC donors and also their cell morphology response to 2, 4, and 6 wt% CA scaffolds. For the rest of this thesis, three BMSC donors were chosen based on their proliferation capacity and CA scaffolds response. While donors 16, 70, and 81 showed the greatest proliferation, cell morphology response to the CA scaffolds was not consistent for donors 16 and 70. Donors 12 and 37 were the next two BMSC donors with highest proliferation capacity. Additionally, they showed a similar and consistent morphology response to the CA scaffolds as donor 81, with BMSC clustering of comparable size. Therefore, donors 12, 37, and 81 were chosen for this study due to their proliferation capacity and similar cell morphology response to the CA scaffolds.

Table 5. Three selected BMSC donors for differentiation study.

| Donor | Sex | Age |
|---|---|---|
| 12 | M | 33 |
| 81 | M | 25 |
| 37 | M | 43 |

## Cell proliferation

In order to assess the proliferation of BMSCs in this study, we performed the Alamar Blue assay in all CA scaffold compositions and 2D substrates at days 2, 7, and 14 of proliferation. Cell numbers are highest in 2D samples than in any scaffold composition at all timepoints. This was

expected since tissue culture plates are treated to promote cell adhesion and proliferation, while CA scaffolds lack adhesion proteins and therefore can lower BMSC proliferation rates.

As can be observed in Figure 13, the main trend among both scaffolds and 2D samples is an increase in cell number, especially apparent at the 14 day timepoint. Among the different scaffold groups, the 2% CA scaffold shows the greatest increase in cell numbers reaching close to 400,000 cells at the fourteen day timepoint. Additionally, donor 81 yields the greatest cell numbers among all BMSC donors after the day 3 timepoint.

The Alamar Blue proliferation assay gave us important insights regarding differences in proliferation within BMSC donors and materials. It is noticeable that there are differences in proliferation capacity between BMSC donors since all samples were seeded with the same cell concentration but yielded different cell numbers at later timepoints. Even when donors 12 and 81 yielded similar cell numbers at the day 3 timepoint in 2% CA and 6% CA samples, this trend was not maintained. Donor 81 yielded much higher cell numbers at later timepoints. Therefore, the Alamar Blue data indicates that there are inherent differences in the proliferation capacity among BMSC donors and confirms our results from the preliminary proliferation study of multiple BMSC donors. Additionally, BMSCs in the 2% CA scaffold reached higher cell numbers than in the 4% CA and 6% CA scaffold compositions. This indicates that there may be a difference in BMSC proliferation capacity with different scaffold stiffnesses.

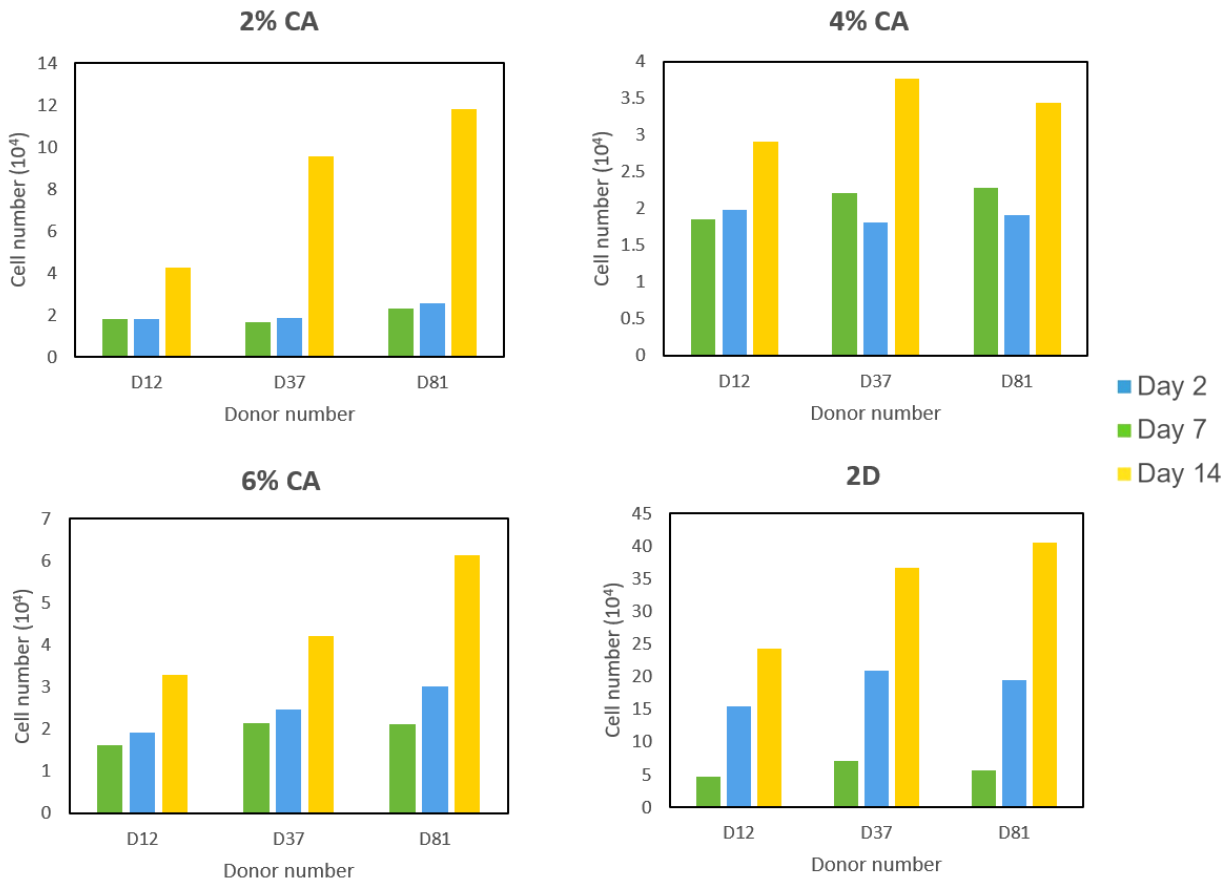


Figure 13. Alamar Blue data for BMSCs in 2, 4, 6 wt% CA and 2D substrates at days 2, 7, and 14.

## Cell Imaging

Cell imaging was performed with the Hoescht 33342 and DiI live fluorescent stains. The Hoescht dye identified the cell nuclei, while the DiI dye helped visualize the cell morphology. At day 3 of proliferation, all BMSC donors clustered into spheroids in the 2, 4, and 6 wt% CA scaffolds while remaining elongated in 2D substrates, as can be observed in Figure 14 which shows overlaid images of both live fluorescent dyes. Bigger spheroids were observed at the higher CA scaffold concentrations (4, 6 wt% CA), while smaller spheroids were seen at the lower CA scaffold

concentrations (2 wt% CA). The BMSC clustering response within the CA scaffolds may be due to its polysaccharide based chemistry and absence of adhesion proteins.

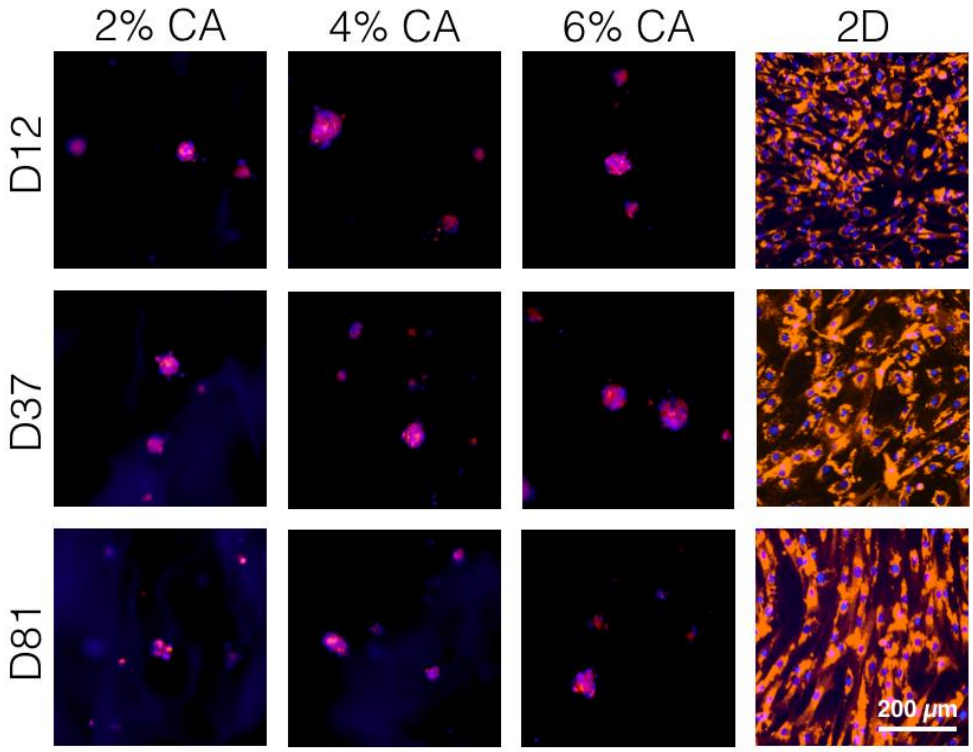


Figure 14. BMSC donors 12, 37, and 81 in 2, 4, 6 wt% CA scaffolds and 2D substrates at day 3 of proliferation were stained Hoechst and DiI live fluorescent dyes.

Similar trends regarding BMSC spheroid size and CA scaffold composition were observed at the 7 and 14 day timepoint as can be observed in Figures 15 and 16, with higher spheroid size corresponding to the stiffer substrates and vice versa. Additionally, cells in 2D substrates remained elongated at all timepoints and increased in confluency. It was also observed that the DiI staining intensity decreased with increasing timepoints, specially in BMSCs seeded on 2D substrates. This occurs since the DiI stain binds to the cell membrane and therefore decreases in concentration as cells undergo division cycles at later timepoints.

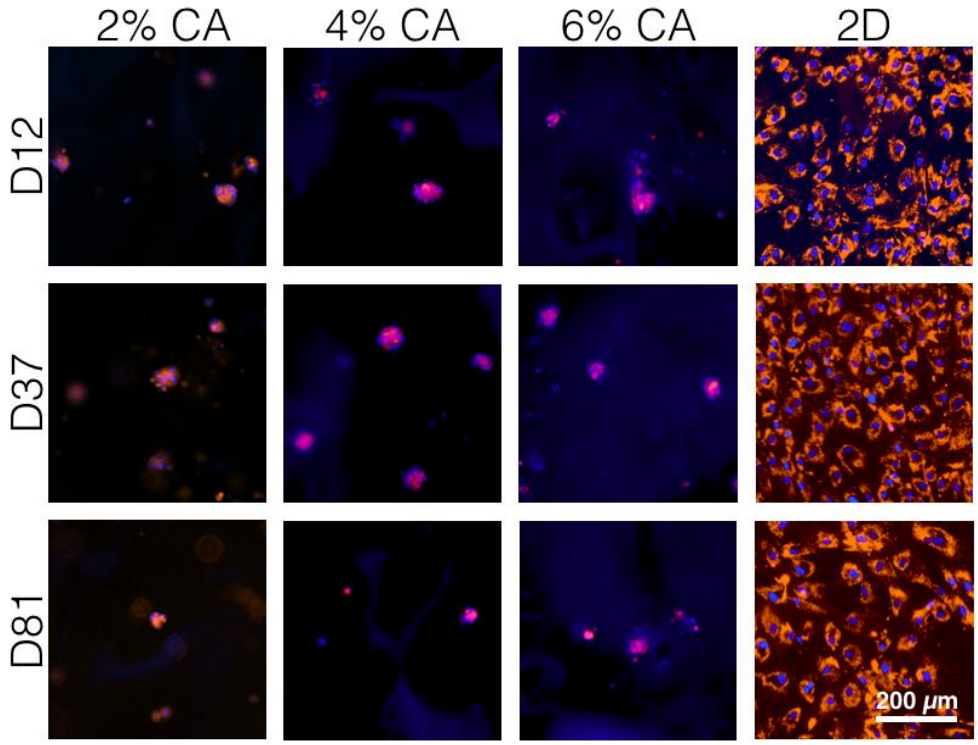

Figure 15. BMSC donors 12, 37, and 81 in 2, 4, 6 wt% CA scaffolds and 2D substrates at day 7 of proliferation were stained Hoechst and DiI live fluorescent dyes.

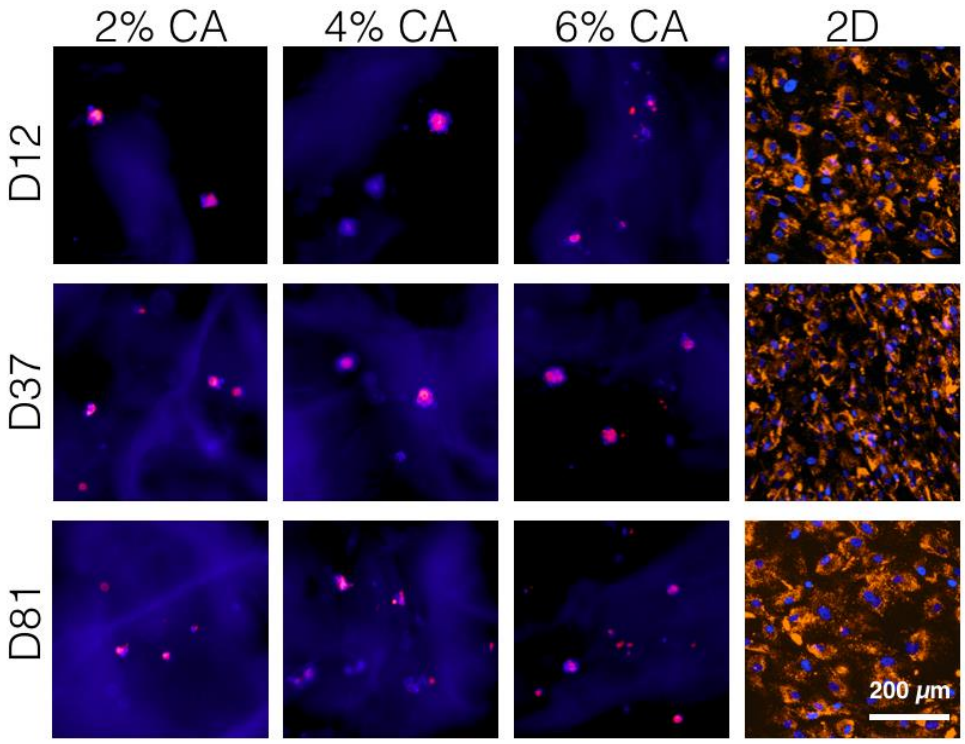


Figure 16. BMSC donors 12, 37, and 81 in 2, 4, 6 wt% CA scaffolds and 2D substrates at day 14 of proliferation were stained Hoechst and DiI live fluorescent dyes.

Spheroid size also varied at different timepoints, as can be seen in Figure 17 for BMSC donor 81 in 2, 4, and 6 wt% CA scaffold at days 3, 7, and 14 of proliferation. The greatest spheroid size was observed at the day 3 timepoint and decreased afterward. These observations were consistent with the preliminary results from the multiple donor BMSC study in Figure 10. We believe decreasing spheroid size could be due to increased cell migration out of the spheroids into the scaffold.

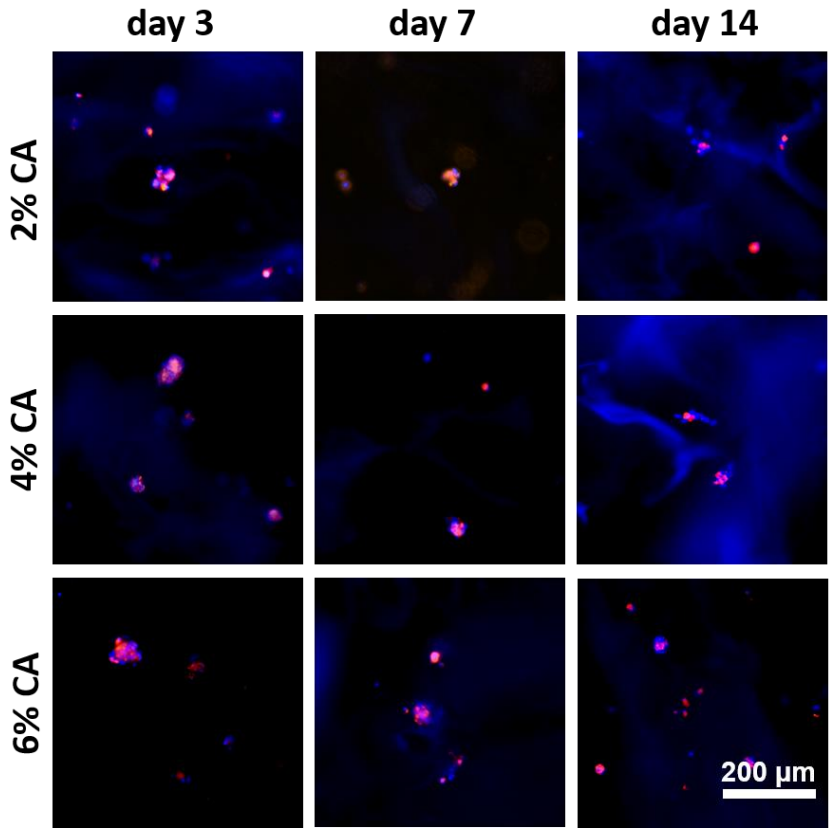

Figure 17. BMSC Donor 81 in 2, 4, 6 wt% CA scaffolds at 3, 7, 14 day timepoints of proliferation.

## Oil Red O and Alizarin Red Staining

### Oil Red O

BMSCs cultured on 2D substrates with adipogenic differentiation medium were stained with Oil Red O dye after 14 and 28 days of differentiation. As can be observed in Figure 18 and 19, the Oil Red O staining solution stains lipid droplets red indicating adipogenic differentiation in BMSCs. Therefore, adipogenic differentiation was achieved in this study among all BMSC donors in the 2D substrates at 14 and 28 days of differentiation.

While adipogenic differentiation occurred among all BMSC donors, the extent of differentiation varied. As can be observed in the lower magnification images of Figures 18 and 19, donor 12 had less positive Oil Red O staining than donor 37 and, similarly, donor 37 had less

positive staining than donor 81. Additionally, the size of the BMSC fat droplets was higher for donor 81 than for donors 12 or 37. Therefore it is not only important to study a single BMSC donor response to a specific substrate or scaffold, but also to look at multiple donor responses since they can give varied results even as control (2D) groups.

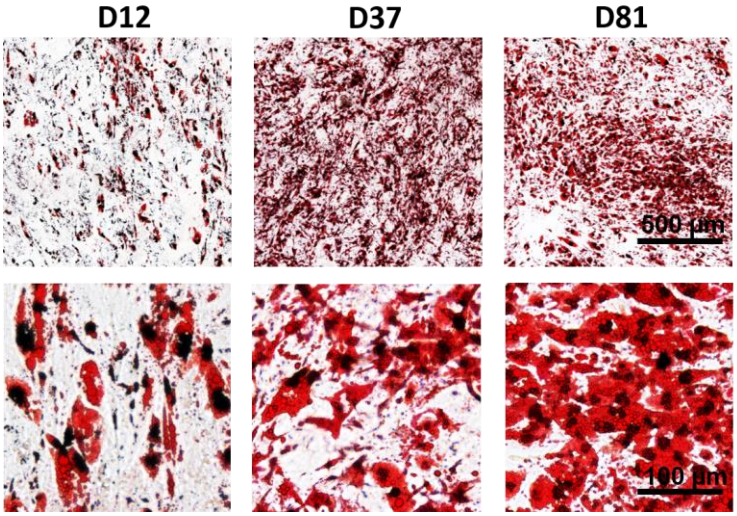


Figure 18. Oil Red O staining on BMSC donors in 2D substrates at 14 days of adipogenic differentiation.

Besides donor variation, differences in the extent of differentiation were also observed at different timepoints. Lipid droplets deposited by BMSCs undergoing adipogenic differentiation are larger in size at the day 28 differentiation timepoint, as can be observed in Figure 19. Greater amounts of lipid deposition by adipocytes at day 28 of differentiation indicate a greater extent of adipogenesis.

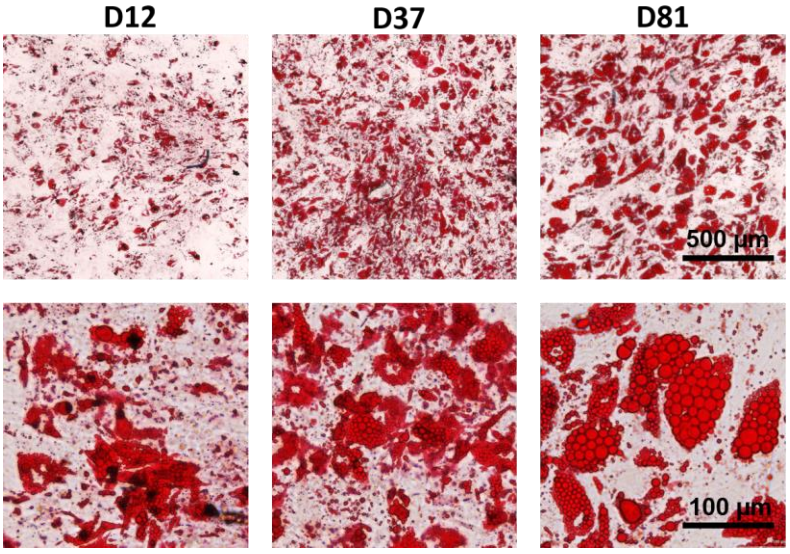


Figure 19. Oil Red O staining on BMSC donors in 2D substrates at 28 days of adipogenic differentiation.

BMSCs cultured in 2, 4, and 6 wt% CA scaffolds under adipogenic differentiation medium were stained with Oil Red O dye after 14 and 28 days of differentiation. Higher magnification images from the 14 and 28 days of differentiation staining can be seen in Figures 20 and 21 respectively, where lipid droplets are stained red in all CA compositions and BMSC donors. Yet, there is a clear distinction in the extent of adipogenic differentiation between materials and donors. Lipid droplets are larger in size in 4 wt% CA and 6 wt% CA materials, while smaller in 2 wt% CA materials. Additionally, donors 37 and 81 showed the largest size of lipid formation which indicates a higher extent of adipogenic differentiation. Overview images of the CA scaffolds for both timepoints are shown in Figures 22 and 23. These images demonstrate the sparse positive staining indicating that higher cell numbers may need to be seeded to support robust adipogenesis.

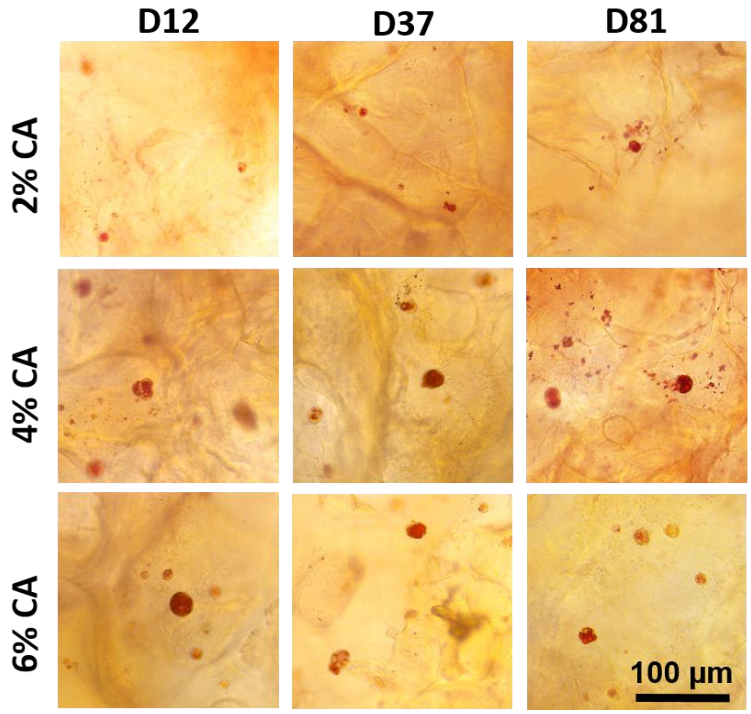


Figure 20. Oil Red O staining in 2, 4, 6% CA scaffolds at 14 days of adipogenic differentiation.

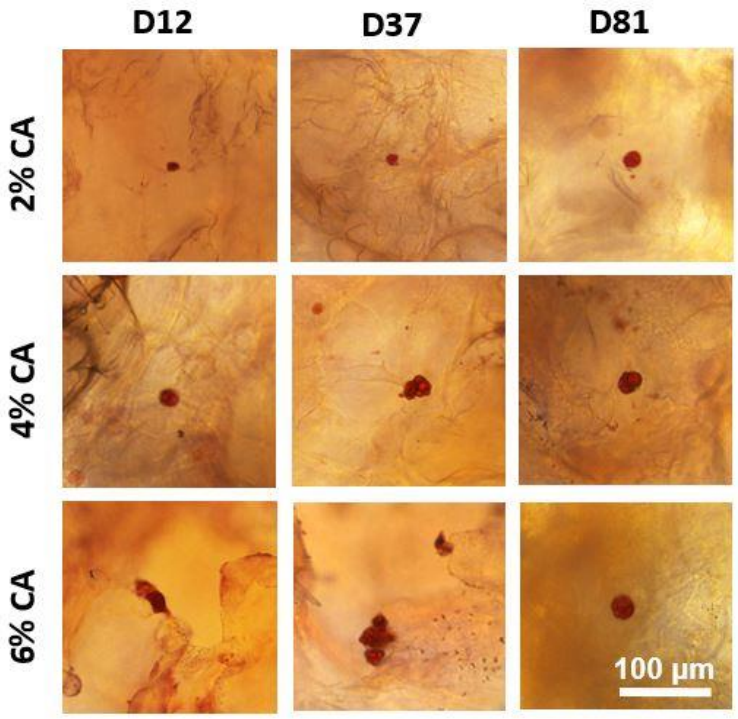


Figure 21. Oil Red O staining in 2, 4, 6% CA scaffolds at 28 days of adipogenic differentiation.

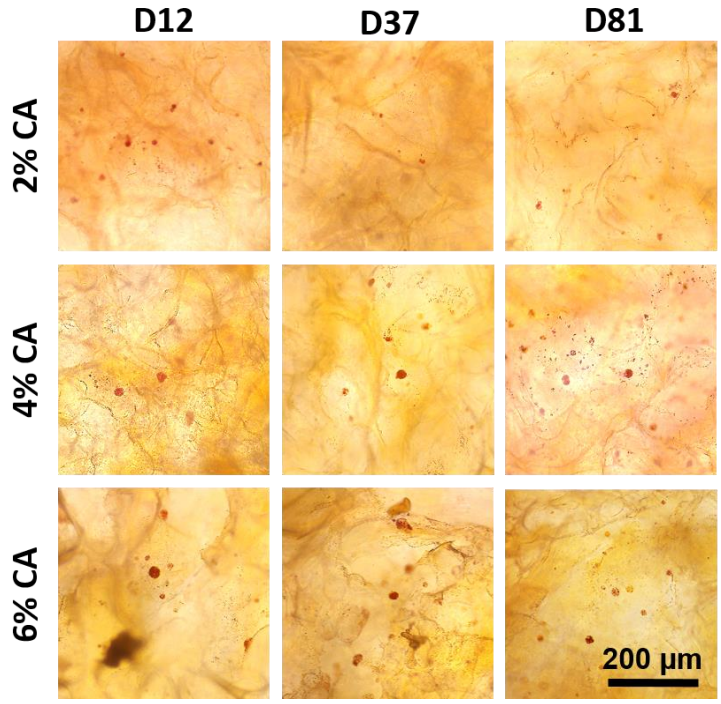

Figure 22. Overview images of Oil Red O staining in 2, 4, 6 wt% CA scaffolds at 14 days of differentiation.

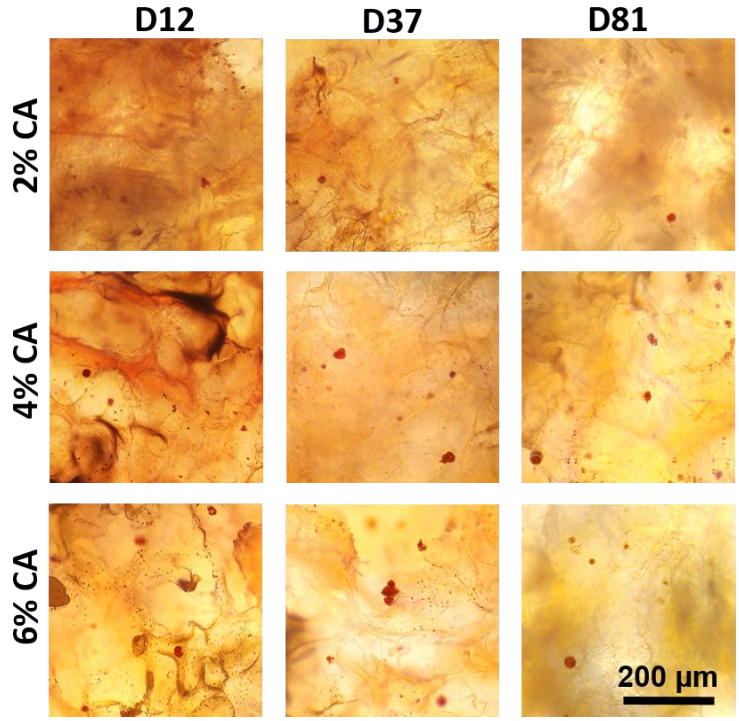

Figure 23. Overview images of Oil Red O staining in 2, 4, 6 wt% CA scaffolds at 28 days of differentiation.

## Alizarin Red

BMSCs cultured on 2D substrates with osteogenic differentiation medium were stained with Alizarin Red dye after 14 and 28 days of differentiation. As can be observed in Figure 24 and 25, the Alizarin Red solution stains calcium deposits in the matrix indicating osteogenic differentiation in BMSCs. Therefore, osteogenic differentiation was achieved in this study among all BMSC donors in the 2D substrates at 14 and 28 days of differentiation.

While osteogenic differentiation occurred among all BMSC donors, the extent of differentiation varied. As can be observed in the overview images of Figures 25, donor 37 showed a greater extent of osteogenic differentiation than donors 12 and 81. Additionally, the extent of osteogenic differentiation increased from day 14 to day 28.

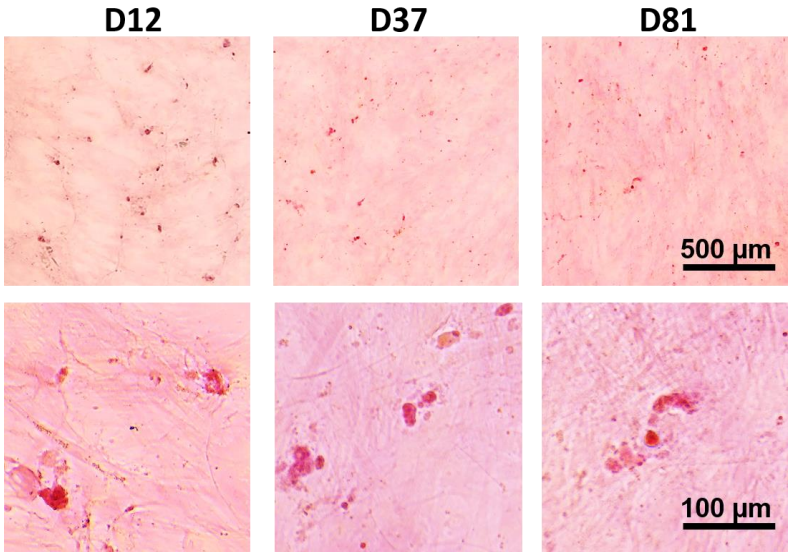


Figure 24. Alizarin Red staining on BMSC donors in 2D at 14 days of osteogenic differentiation.

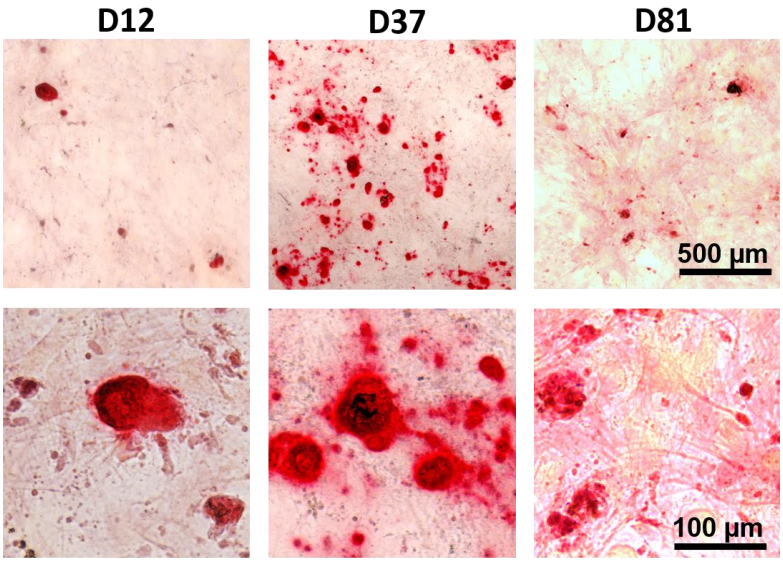


Figure 25. Alizarin Red staining on BMSC donors in 2D at 28 days of osteogenic differentiation.

BMSC samples cultured in 2, 4, and 6 wt% CA scaffolds under osteogenic differentiation medium were stained with Alizarin Red dye after 14 and 28 days of differentiation. In Figure 26, we can observe overview images for 2, 4, and 6 wt% CA samples at 14 days of osteogenic differentiation media treatment. The positive red stain indicates osteogenic differentiation among all donors and CA scaffold samples. Moreover, the darker spots indicate bone nodule formation due to matrix mineralization. In day 14 samples, matrix mineralization was higher for samples in stiffer substrates (4, 6 wt% CA) in comparison to softer substrates (2 wt% CA).

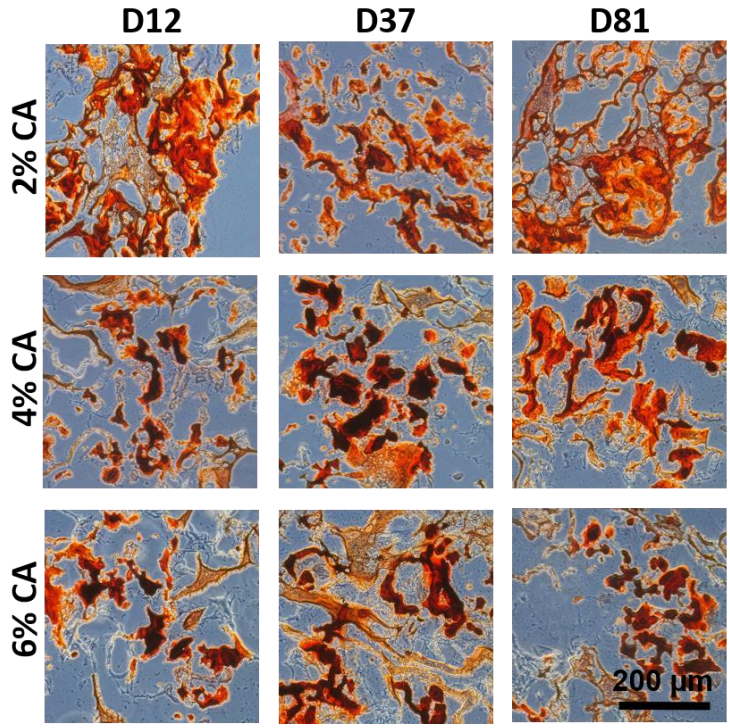

Figure 26. BMSC donors in 2, 4, 6 wt% CA scaffolds were stained with Alizarin Red after 14 days of osteogenic differentiation.

BMSC samples at 28 days of osteogenic differentiation were also processed for histology and stained with Alizarin Red solution to analyze the extent of mineralization as can be observed in Figure 27. Similarly to the day 14 differentiation results, all scaffold samples and BMSC donors stained positively for osteogenic differentiation with Alizarin Red. 4 wt% CA and 6 wt% CA samples exhibited greater matrix mineralization than 2 wt% CA samples indicated by bone nodule formation. These results support our initial hypothesis, where stiffer substrates support greater BMSC osteogenic differentiation and matrix mineralization. Higher magnification images for both days 14 and 28 of osteogenic differentiation can be found in Figures 28 and 29, which more clearly show nodule formation from calcium deposits in the scaffold. Greater mineralization at higher CA scaffold stiffnesses supports that BMSC osteogenic differentiation is influenced by substrate mechanical properties and that cell material interactions guide BMSC cell fate.

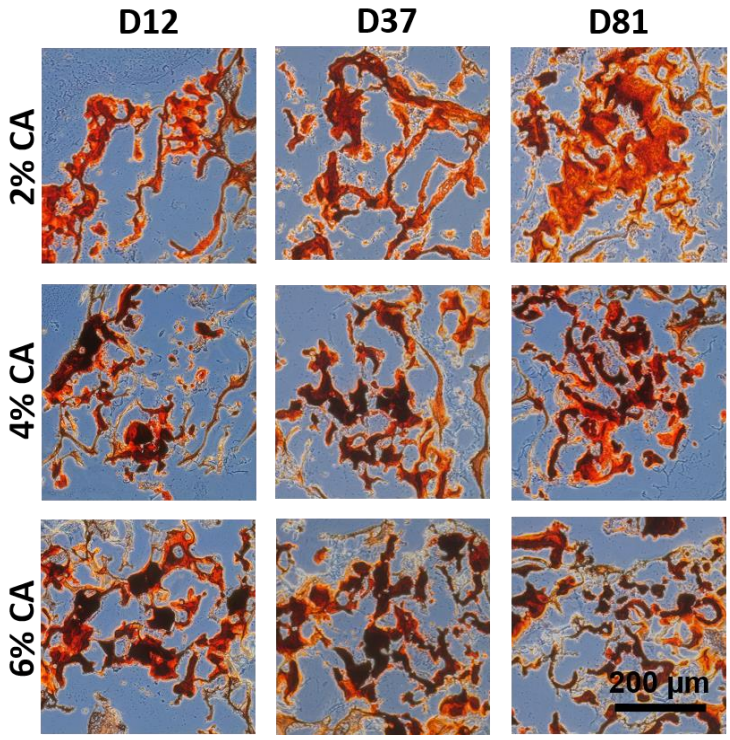

Figure 27. BMSC donors in 2, 4, 6 wt% CA scaffolds were stained with Alizarin Red after 28 days of osteogenic differentiation.

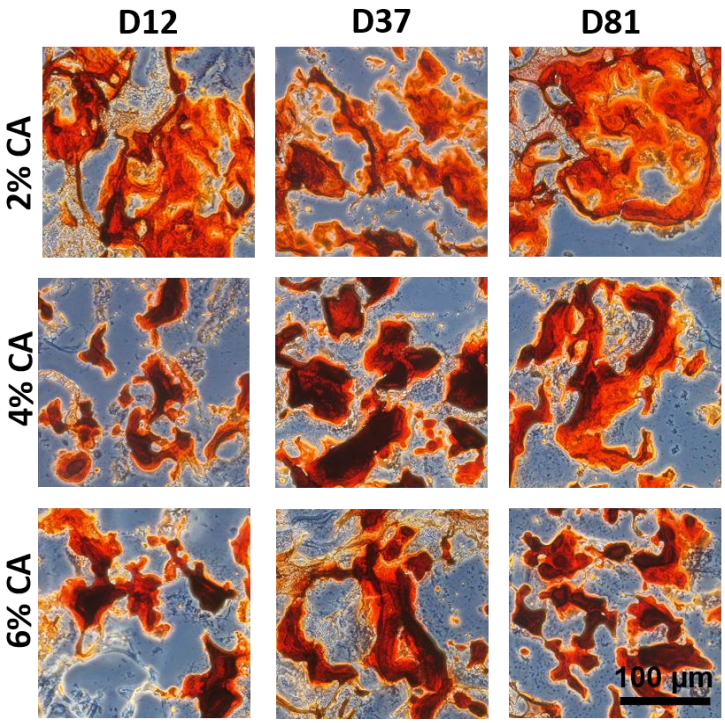

Figure 28. High magnification images of BMSC donors in 2, 4, 6 wt% CA scaffolds were stained with Alizarin Red after 14 days of osteogenic differentiation.

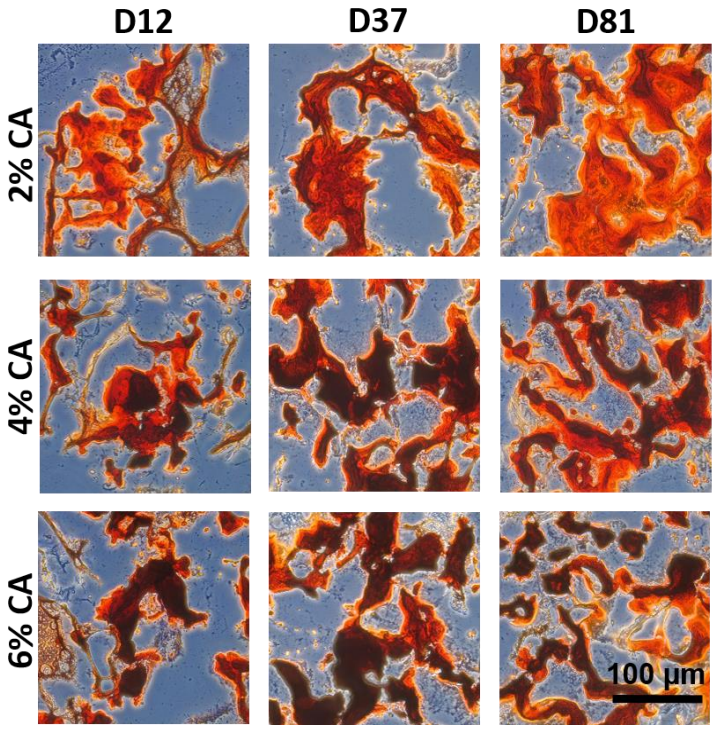

Figure 29. High magnification images of BMSC donors in 2, 4, 6 wt% CA scaffolds were stained with Alizarin Red after 28 days of osteogenic differentiation

# CHAPTER 5: CONCLUSIONS

This thesis examined the effects of CA scaffold stiffness variation on BMSC adipogenic and osteogenic differentiation. An array of CA scaffolds (2, 4, 6 wt% CA) was produced by varying the polymer concentrations. CA scaffolds were fabricated by freeze casting and lyophilization to yield an interconnected porous structure. The CA porous scaffold array had different mechanical properties but the same chemical composition.

In order to characterize the CA scaffold properties, SEM, compression mechanical testing, and FTIR were performed. SEM images and average pore size calculations demonstrated decreasing pore sizes at higher CA scaffold concentrations. Compression mechanical testing yielded higher elastic moduli values for higher CA scaffold concentrations in both dry and wet conditions, with wet conditions giving values two orders of magnitude lower than dry conditions. FTIR data demonstrated the formation of PECs at all CA scaffold compositions.

Three BMSC donors were seeded on the CA scaffold array to examine the cell response to different scaffold stiffnesses and BMSC donor variation. The cell culture study included a 14 day proliferation phase, followed by 28 days of differentiation under adipogenic or osteogenic differentiation media. The Alamar Blue proliferation assay showed an increase in cell number at the 14 day timepoint for all CA scaffold compositions and BMSC donors. BMSC donors 37 and 81 showed higher cell numbers than donor 12 at most timepoints in the alamar blue assay. BMSCs formed spheroids in all CA scaffold compositions, with higher stiffnesses (4, 6 wt% CA) promoting larger spheroid formation than lower stiffnesses (2 wt% CA). Spheroid size for all CA scaffold compositions and BMSC donors decreased after day 3 of proliferation possibly due to cell migration in the scaffold.

After 28 days of adipogenic differentiation, BMSCs in CA scaffolds and 2D samples were stained with Oil Red O dye to target lipid droplets indicating adipogenic commitment. In 2D samples, the largest positive Oil Red O staining was observed for donor 81, followed by donors 37 and 12 respectively. In the CA scaffold array, the greatest Oil Red staining was observed for donors 37 and 81 in the 4 and 6 wt% CA scaffolds.

While positive Oil Red O staining was observed for all scaffold compositions, more robust differentiation was expected at the lower CA scaffold concentrations (2 wt% CA). Therefore this study disproved our hypothesis for the adipogenic differentiation group. The polysaccharide composition of the CA scaffolds likely contributed to the spheroid formation and influenced the extent of differentiation. It can be noted that the largest adipogenic differentiation was observed in scaffolds that yielded the largest cell clusters (4, 6 wt%).

The extent of osteogenic differentiation was also assessed for BMSCs in CA scaffolds and 2D samples with Alizarin Red dye to target calcium deposits indicating osteogenic differentiation. In 2D samples, the largest Alizarin Red staining was observed for donor 37. Additionally, the extent of osteogenic differentiation increased from day 14 to day 28 among all BMSC donors. In the CA scaffolds, all compositions stained positively for osteogenic differentiation at both day 14 and day 28 of differentiation. Stiffer substrates (4, 6 wt% CA) exhibited greater mineralization than softer substrates (2 wt% CA) indicated by matrix darkening, also called bone nodule formation, surrounded by positive Alizarin Red staining. While all CA compositions and BMSC donors supported osteogenic differentiation, scaffolds with higher stiffnesses showed a greater extent of osteogenic differentiation indicated by matrix mineralization. Therefore, samples treated for osteogenic differentiation supported our initial hypothesis that stiffer scaffold substrates would further guide BMSCs towards osteogenic lineage differentiation.

For both adipogenic and osteogenic differentiation, the greatest extent of differentiation occurred in the 4 and 6 wt% CA scaffolds relative to the 2 wt% CA scaffolds. These scaffold compositions also formed the largest cell spheroids, which studies have associated with stemness markers [85]. It is possible that 4 and 6 wt% CA scaffolds helped maintain BMSC stemness during the proliferation phase indicated by the larger cell clusters, which could contribute to a greater extent of differentiation. Further optimization of the CA scaffolds will be needed in order to examine the effects of scaffold stiffness independently of the effects of polysaccharide chemistry and spheroid formation on BMSC differentiation. Protein based coatings could be adsorbed onto the CA scaffolds to enhance BMSC adhesion, proliferation, and differentiation, while changing the cell morphology from a spherical to an elongated shape. Additionally, increasing scaffold cell density could potentially yield more robust differentiation.

# APPENDIX A: BMSC DONOR 81 STANDARD CURVE FOR ALAMAR BLUE ASSAY

A)

| Intensity | Cell Number |
|---|---|
| 0 | 0 |
| 416.5 | 50000 |
| 654.25 | 100000 |
| 1075.75 | 200000 |
| 2567.25 | 500000 |
| 3954.5 | 1000000 |
| 4614.75 | 1500000 |

B)

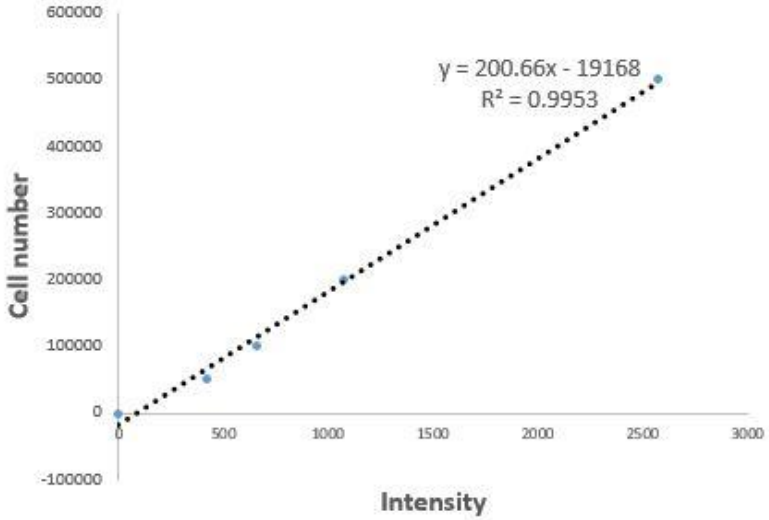


(A) List of intensity readings from the Alamar Blue assay at different cell numbers from 0 to 1.5 million. Blank readings were subtracted from these intensity values.

(B) Standard curve generated from the trendline of cell number and intensity values.

# APPENDIX B: OVERVIEW IMAGES OF BMSCS IN CA SCAFFOLD SAMPLES AT DAYS 3, 7, AND 14 OF PROLIFERATION

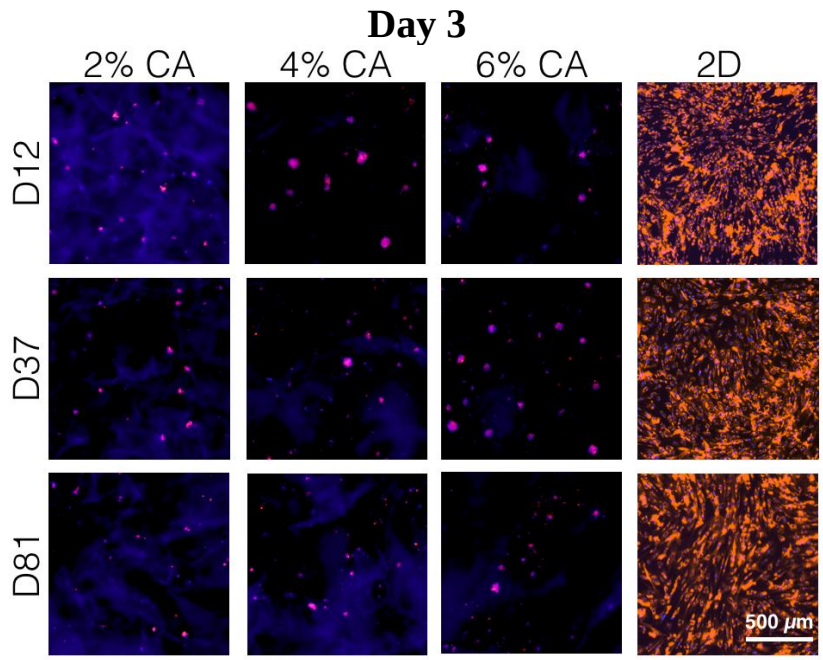


DiI and Hoescht stains at day 3 of proliferation for BMSC donors seeded on 2, 4, 6 wt% CA scaffolds.

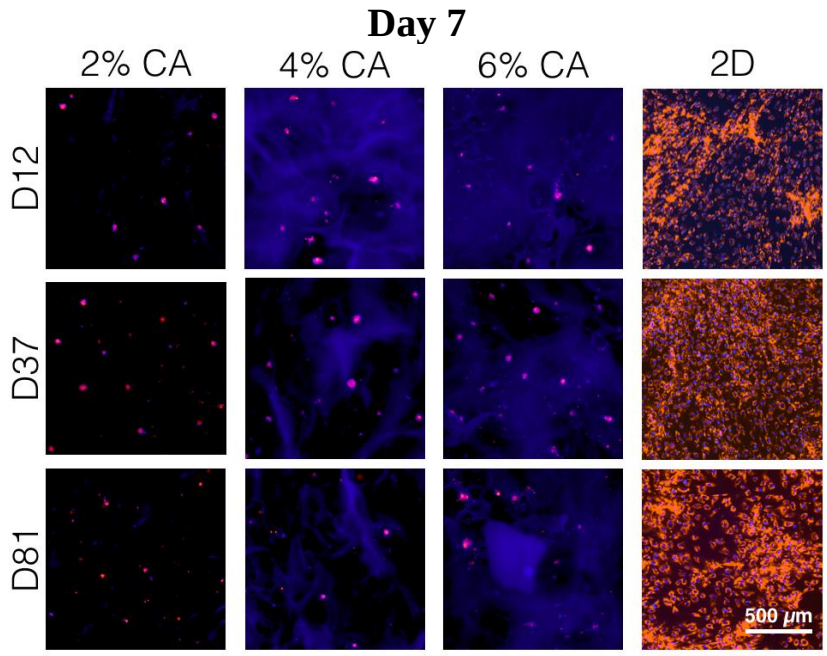


DiI and Hoescht stains at day 7 of proliferation for BMSC donors seeded on 2, 4, 6 wt% CA scaffolds.

## Day 14

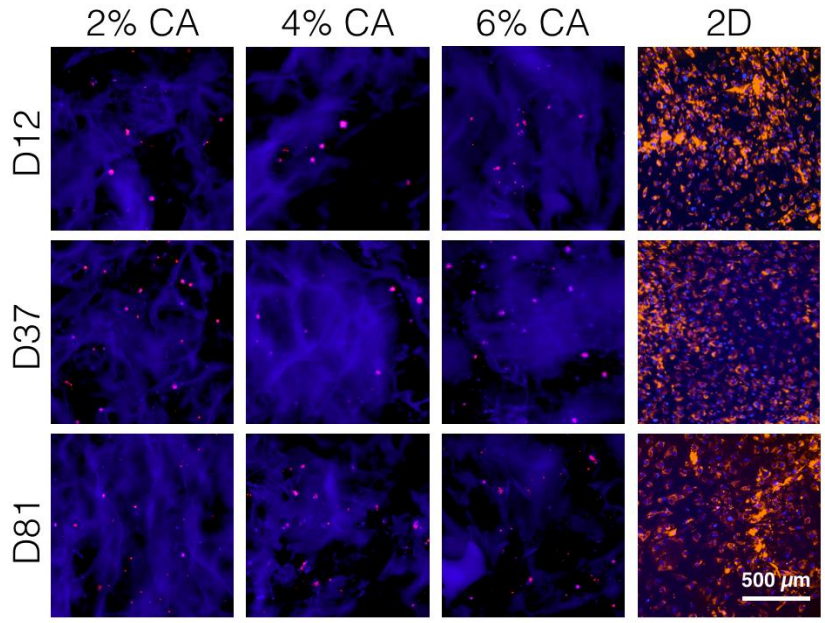


DiI and Hoescht stains at day 14 of proliferation for BMSC donors seeded on 2, 4, 6 wt% CA scaffolds.

# APPENDIX C: ALIZARIN RED CONTROL STAINING OF 2, 4, 6 WT% CA SCAFFOLDS WITHOUT BMSCS

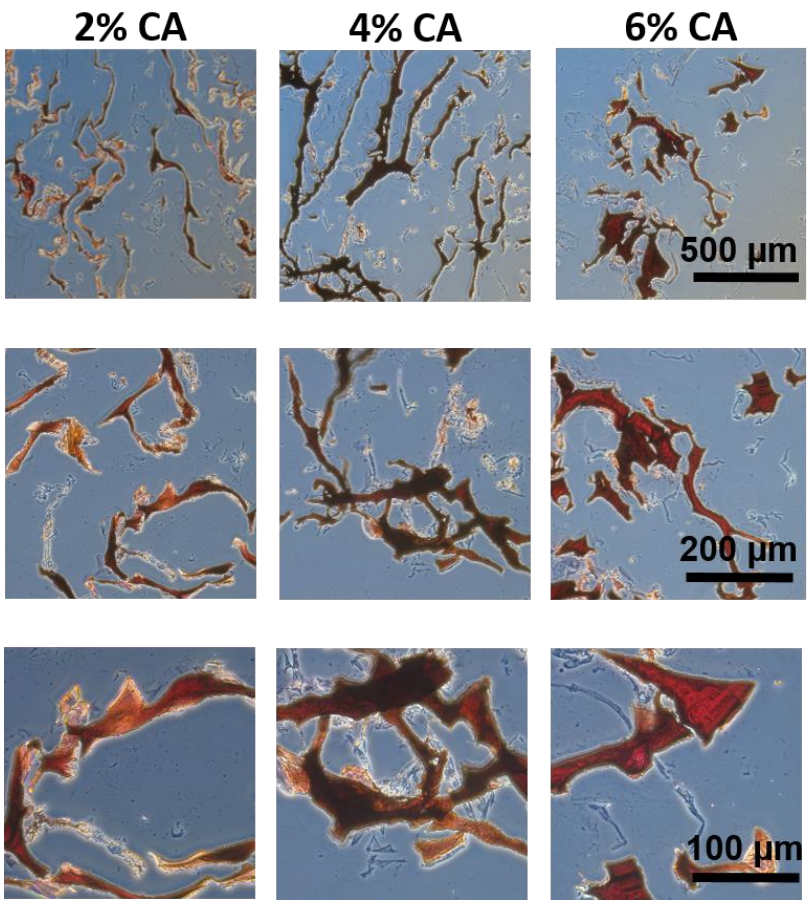


Control staining of Alizarin Red solution in 2, 4, 6 wt% CA scaffolds without BMSCs crosslinked, sterilized, and processed for histology.

# LIST OF REFERENCES


[1] Z. Li, H. R. Ramay, K. D. Hauch, D. Xiao, and M. Zhang, "Chitosan-alginate hybrid scaffolds for bone tissue engineering," *Biomaterials*, vol. 26, no. 18, pp. 3919–3928, 2005.

[2] S. J. Florczyk, M. Leung, Z. Li, J. I. Huang, R. A. Hopper, and M. Zhang, "Evaluation of three-dimensional porous chitosan-alginate scaffolds in rat calvarial defects for bone regeneration applications," *J. Biomed. Mater. Res. - Part A*, vol. 101, no. 10, pp. 2974–2983, 2013.

[3] A. Vajgel, N. Mardas, B. C. Farias, A. Petrie, R. Cimões, and N. Donos, "A systematic review on the critical size defect model," *Clin. Oral Implants Res.*, vol. 25, no. 8, pp. 879–893, 2014.

[4] T. S. Bentley and S. G. Hanson, "2017 U.S. organ and tissue transplant cost estimates and discussion," *Milliman Res. Rep.*, no. April, pp. 1–16, 2011.

[5] B. M. Roux, M. H. Cheng, and E. M. Brey, "Engineering clinically relevant volumes of vascularized bone," *J. Cell. Mol. Med.*, vol. 19, no. 5, pp. 903–914, 2015.

[6] A. Ebrahimi, S. A. Hosseini, and F. Rahim, "Immunosuppressive therapy in allograft transplantation: From novel insights and strategies to tolerance and challenges," *Central European Journal of Immunology*, vol. 39, no. 3. pp. 400–409, 2014.

[7] D. F. Williams, *Definitions in biomaterials: proceedings of a consensus conference of the European Society for Biomaterials*. Elsevier, 1987.

[8] B. D. Ratner, A. S. Hoffman, F. J. Schoen, and J. Lemons, *Biomaterials Science : A Multidisciplinary Endeavor*. Academic Press, 2004.

[9] F. Khan and S. R. Ahmad, "Polysaccharides and Their Derivatives for Versatile Tissue

Engineering Application," *Macromolecular Bioscience*, vol. 13, no. 4. pp. 395–421, 2013.

[10] B. S. Kim and D. J. Mooney, "Development of biocompatible synthetic extracellular matrices for tissue engineering," *Trends in Biotechnology*, vol. 16, no. 5. pp. 224–229, 1998.

[11] B. Dhandayuthapani, Y. Yoshida, T. Maekawa, and D. S. Kumar, "Polymeric scaffolds in tissue engineering application: A review," *International Journal of Polymer Science*, vol. 2011. 2011.

[12] N. Mohan and P. D. Nair, "Novel porous, polysaccharide scaffolds for tissue engineering applications," *Trends Biomater. Artif. Organs*, vol. 18, no. 2, pp. 219–224, 2005.

[13] A. Khademhosseini and R. Langer, "A decade of progress in tissue engineering," *Nat. Protoc.*, vol. 11, no. 10, pp. 1775–1781, 2016.

[14] A. I. Caplan, "Adult mesenchymal stem cells for tissue engineering versus regenerative medicine," *Journal of Cellular Physiology*, vol. 213, no. 2. pp. 341–347, 2007.

[15] P. Robey, "'Mesenchymal stem cells': fact or fiction, and implications in their therapeutic use," *F1000Research*, vol. 6, p. 524, 2017.

[16] A. J. Rosenbaum, D. A. Grande, and J. S. Dines, "The use of mesenchymal stem cells in tissue engineering: A global assessment," *Organogenesis*, vol. 4, no. 1. pp. 23–27, 2008.

[17] B. Levi and M. T. Longaker, "Concise review: adipose-derived stromal cells for skeletal regenerative medicine.," *Stem Cells*, vol. 29, no. 4, pp. 576–82, 2011.

[18] M. M. Bonab, K. Alimoghaddam, F. Talebian, S. H. Ghaffari, A. Ghavamzadeh, and B. Nikbin, "Aging of mesenchymal stem cell in vitro," *BMC Cell Biol.*, vol. 7, 2006.

[19] J. Lo Surdo and S. R. Bauer, "Quantitative Approaches to Detect Donor and Passage Differences in Adipogenic Potential and Clonogenicity in Human Bone Marrow-Derived

Mesenchymal Stem Cells," *Tissue Eng. Part C Methods*, vol. 18, no. 11, pp. 877–889, 2012.

[20] A. Rupani, R. Balint, and S. H. Cartmell, "Osteoblasts and their applications in bone tissue engineering," *Cell Health and Cytoskeleton*, vol. 4. pp. 49–61, 2012.

[21] C. G. Bellows, J. N. M. Heersche, and J. E. Aubin, "Determination of the capacity for proliferation and differentiation of osteoprogenitor cells in the presence and absence of dexamethasone," *Dev. Biol.*, vol. 140, no. 1, pp. 132–138, 1990.

[22] C. H. Chung, E. E. Golub, E. Forbes, T. Tokuoka, and I. M. Shapiro, "Mechanism of action of beta-glycerophosphate on bone cell mineralization.," *Calcif. Tissue Int.*, vol. 51, no. 4, pp. 305–311, 1992.

[23] G. R. Beck, B. Zerler, and E. Moran, "Phosphate is a specific signal for induction of osteopontin gene expression," *Proc. Natl. Acad. Sci.*, vol. 97, no. 15, pp. 8352–8357, 2000.

[24] T. Fujita *et al.*, "Phosphate provides an extracellular signal that drives nuclear export of Runx2/Cbfa1 in bone cells," *Biochem. Biophys. Res. Commun.*, vol. 280, no. 1, pp. 348–352, 2001.

[25] N. W. Marion and J. J. Mao, "Mesenchymal Stem Cells and Tissue Engineering," *Methods in Enzymology*, vol. 420. pp. 339–361, 2006.

[26] A. Asti and L. Gioglio, "Natural and synthetic biodegradable polymers: Different scaffolds for cell expansion and tissue formation," *International Journal of Artificial Organs*, vol. 37, no. 3. pp. 187–205, 2014.

[27] M. Tencerova and M. Kassem, "The bone marrow-derived stromal cells: Commitment and regulation of adipogenesis," *Frontiers in Endocrinology*, vol. 7, no. SEP. 2016.

[28] R. Vishnubalaji, M. Al-Nbaheen, B. Kadalmani, A. Aldahmash, and T. Ramesh, "Comparative investigation of the differentiation capability of bone-marrow- and adipose-derived mesenchymal stem cells by qualitative and quantitative analysis," *Cell Tissue Res.*, vol. 347, no. 2, pp. 419–427, 2012.

[29] M. F. Pittenger, "Multilineage Potential of Adult Human Mesenchymal Stem Cells," *Science (80-. ).*, vol. 284, no. 5411, pp. 143–147, 1999.

[30] J. H. Choi *et al.*, "Adipose Tissue Engineering for Soft Tissue Regeneration," *Tissue Eng. Part B Rev.*, vol. 16, no. 4, pp. 413–426, 2010.

[31] G. C. Reilly and A. J. Engler, "Intrinsic extracellular matrix properties regulate stem cell differentiation," *J. Biomech.*, vol. 43, no. 1, pp. 55–62, 2010.

[32] K. A. Jansen, P. Atherton, and C. Ballestrem, "Mechanotransduction at the cell-matrix interface," *Seminars in Cell and Developmental Biology*, vol. 71. pp. 75–83, 2017.

[33] R. O. Hynes, "Integrins: Versatility, modulation, and signaling in cell adhesion," *Cell*, vol. 69, no. 1. pp. 11–25, 1992.

[34] H. Lv *et al.*, "Mechanism of regulation of stem cell differentiation by matrix stiffness," *Stem Cell Res. Ther.*, vol. 6, no. 1, p. 103, 2015.

[35] Y. Mao and J. E. Schwarzbauer, "Fibronectin fibrillogenesis, a cell-mediated matrix assembly process," *Matrix Biology*, vol. 24, no. 6. pp. 389–399, 2005.

[36] A. J. Engler, S. Sen, H. L. Sweeney, and D. E. Discher, "Matrix Elasticity Directs Stem Cell Lineage Specification," *Cell*, vol. 126, no. 4, pp. 677–689, 2006.

[37] B. D. Ratner, A. S. Hoffman, F. J. Schoen, and J. E. Lemons, *Biomaterials science: an introduction to materials in medicine*. 2004.

[38] M. E. Chicurel, R. H. Singer, C. J. Meyer, and D. E. Ingber, "Integrin binding and

mechanical tension induce movement of mRNA and ribosomes to focal adhesions," *Nature*, vol. 392, no. 6677, pp. 730–733, 1998.

[39] M. M. Martino, M. Mochizuki, D. A. Rothenfluh, S. A. Rempel, J. A. Hubbell, and T. H. Barker, "Controlling integrin specificity and stem cell differentiation in 2D and 3D environments through regulation of fibronectin domain stability," *Biomaterials*, vol. 30, no. 6, pp. 1089–1097, 2009.

[40] A. Katsumi, T. Naoe, T. Matsushita, K. Kaibuchi, and M. A. Schwartz, "Integrin activation and matrix binding mediate cellular responses to mechanical stretch," *J. Biol. Chem.*, vol. 280, no. 17, pp. 16546–16549, 2005.

[41] J. M. Curran, R. Chen, and J. A. Hunt, "The guidance of human mesenchymal stem cell differentiation in vitro by controlled modifications to the cell substrate," *Biomaterials*, vol. 27, no. 27, pp. 4783–4793, 2006.

[42] A. J. Engler, M. Chan, D. Boettiger, and J. E. Schwarzbauer, "A novel mode of cell detachment from fibrillar fibronectin matrix under shear," *J. Cell Sci.*, vol. 122, no. 10, pp. 1647–1653, 2009.

[43] C. M. Williams, A. J. Engler, R. D. Slone, L. L. Galante, and J. E. Schwarzbauer, "Fibronectin expression modulates mammary epithelial cell proliferation during acinar differentiation," *Cancer Res.*, vol. 68, no. 9, pp. 3185–3192, 2008.

[44] P. J. Wipff, D. B. Rifkin, J. J. Meister, and B. Hinz, "Myofibroblast contraction activates latent TGF-β1 from the extracellular matrix," *J. Cell Biol.*, vol. 179, no. 6, pp. 1311–1323, 2007.

[45] F. Khan and M. Tanaka, "Designing smart biomaterials for tissue engineering," *Int. J. Mol. Sci.*, vol. 19, no. 1, 2018.

[46] L. Ma *et al.*, “Collagen/chitosan porous scaffolds with improved biostability for skin tissue engineering,” *Biomaterials*, vol. 24, no. 26, pp. 4833–4841, 2003.

[47] D. W. Hutmacher, “Scaffolds in tissue engineering bone and cartilage,” *Biomaterials*, vol. 21, no. 24, pp. 2529–2543, 2000.

[48] J. Mayer, E. Karamuk, T. Akaike, and E. Wintermantel, “Matrices for tissue engineering-scaffold structure for a bioartificial liver support system,” in *Journal of Controlled Release*, 2000, vol. 64, no. 1–3, pp. 81–90.

[49] G. C. Engelmayr, M. Cheng, C. J. Bettinger, J. T. Borenstein, R. Langer, and L. E. Freed, “Accordion-like honeycombs for tissue engineering of cardiac anisotropy,” *Nat. Mater.*, vol. 7, no. 12, pp. 1003–1010, 2008.

[50] E. Tziampazis and A. Sambanis, “Tissue Engineering of a Bioartificial Pancreas: Modeling the Cell Environment and Device Function,” *Biotechnol. Prog.*, vol. 11, no. 2, pp. 115–126, 1995.

[51] F. Oberpenning, J. Meng, J. J. Yoo, and A. Atala, “De novo reconstitution of a functional mammalian urinary bladder by tissue engineering,” *Nat. Biotechnol.*, vol. 17, no. 2, pp. 149–155, 1999.

[52] B. D. Lawrence, J. K. Marchant, M. A. Pindrus, F. G. Omenetto, and D. L. Kaplan, “Silk film biomaterials for cornea tissue engineering,” *Biomaterials*, vol. 30, no. 7, pp. 1299–1308, 2009.

[53] M. P. Lutolf and J. A. Hubbell, “Synthetic biomaterials as instructive extracellular microenvironments for morphogenesis in tissue engineering,” *Nature Biotechnology*, vol. 23, no. 1. pp. 47–55, 2005.

[54] M. I. Sabir, X. Xu, and L. Li, “A review on biodegradable polymeric materials for bone

tissue engineering applications," *J. Mater. Sci.*, vol. 44, no. 21, pp. 5713–5724, 2009.

[55] P. A. Gunatillake, R. Adhikari, and N. Gadegaard, "Biodegradable synthetic polymers for tissue engineering," *European Cells and Materials*, vol. 5. pp. 1–16, 2003.

[56] Z. Li and J. Guan, "Hydrogels for cardiac tissue engineering," *Polymers*, vol. 3, no. 2. pp. 740–761, 2011.

[57] F. Wen, S. Chang, Y. C. Toh, S. H. Teoh, and H. Yu, "Development of poly (lactic-co-glycolic acid)-collagen scaffolds for tissue engineering," *Mater. Sci. Eng. C*, vol. 27, no. 2, pp. 285–292, 2007.

[58] P. X. Ma, "Scaffolds for tissue fabrication," *Materials Today*, vol. 7, no. 5. pp. 30–40, 2004.

[59] L. S. Nair and C. T. Laurencin, "Biodegradable polymers as biomaterials," *Progress in Polymer Science (Oxford)*, vol. 32, no. 8–9. pp. 762–798, 2007.

[60] C. Yang *et al.*, "The application of recombinant human collagen in tissue engineering," *BioDrugs*, vol. 18, no. 2. pp. 103–119, 2004.

[61] U. Cheema, M. Ananta, and V. Muder, "Collagen: Applications of a Natural Polymer in Regenerative Medicine," in *Regenerative Medicine and Tissue Engineering - Cells and Biomaterials*, 2011.

[62] X. H. Zhu, Y. Tabata, C.-H. Wang, and Y. W. Tong, "Delivery of basic fibroblast growth factor from gelatin microsphere scaffold for the growth of human umbilical vein endothelial cells.," *Tissue Eng. Part A*, vol. 14, no. 12, pp. 1939–47, 2008.

[63] C. Tondera *et al.*, "Gelatin-based hydrogel degradation and tissue interaction in vivo: Insights from multimodal preclinical imaging in immunocompetent nude mice," *Theranostics*, vol. 6, no. 12, pp. 2114–2128, 2016.

[64] M. Rajkumar, K. Kavitha, M. Prabhu, N. Meenakshisundaram, and V. Rajendran, "Nanohydroxyapatite-chitosan-gelatin polyelectrolyte complex with enhanced mechanical and bioactivity," *Mater. Sci. Eng. C*, vol. 33, no. 6, pp. 3237–3244, 2013.

[65] B. B. Mandal, A. Grinberg, E. S. Gil, B. Panilaitis, and D. L. Kaplan, "High-strength silk protein scaffolds for bone repair.," *Proc. Natl. Acad. Sci. U. S. A.*, vol. 109, no. 20, pp. 7699–704, 2012.

[66] P. B. Malafaya, G. A. Silva, and R. L. Reis, "Natural-origin polymers as carriers and scaffolds for biomolecules and cell delivery in tissue engineering applications," *Advanced Drug Delivery Reviews*, vol. 59, no. 4–5. pp. 207–233, 2007.

[67] N. Bhardwaj and S. C. Kundu, "Silk fibroin protein and chitosan polyelectrolyte complex porous scaffolds for tissue engineering applications," *Carbohydr. Polym.*, vol. 85, no. 2, pp. 325–333, 2011.

[68] A. C. Brown and T. H. Barker, "Fibrin-based biomaterials: Modulation of macroscopic properties through rational design at the molecular level," *Acta Biomaterialia*, vol. 10, no. 4. pp. 1502–1514, 2014.

[69] T. A. E. Ahmed, E. V. Dare, and M. Hincke, "Fibrin: a versatile scaffold for tissue engineering applications," *Tissue Eng. Part B Rev.*, vol. 14, no. 2, pp. 199–215, 2008.

[70] N. B. Shelke, R. James, C. T. Laurencin, and S. G. Kumbar, "Polysaccharide biomaterials for drug delivery and regenerative engineering," *Polymers for Advanced Technologies*, vol. 25, no. 5. pp. 448–460, 2014.

[71] T. Jiang, S. G. Kumbar, L. S. Nair, and C. T. Laurencin, "Biologically active chitosan systems for tissue engineering and regenerative medicine.," *Curr. Top. Med. Chem.*, vol. 8, pp. 354–364, 2008.

[72] J. Berger, M. Reist, J. M. Mayer, O. Felt, N. A. Peppas, and R. Gurny, “Structure and interactions in covalently and ionically crosslinked chitosan hydrogels for biomedical applications,” *European Journal of Pharmaceutics and Biopharmaceutics*, vol. 57, no. 1. pp. 19–34, 2004.

[73] K. Y. Lee and D. J. Mooney, “Alginate: properties and biomedical applications.,” *Prog. Polym. Sci.*, vol. 37, no. 1, pp. 106–126, 2012.

[74] M. C. Straccia, G. G. D’Ayala, I. Romano, A. Oliva, and P. Laurienzo, “Alginate hydrogels coated with chitosan for wound dressing,” *Mar. Drugs*, vol. 13, no. 5, pp. 2890–2908, 2015.

[75] N. Huebsch *et al.*, “Harnessing traction-mediated manipulation of the cell/matrix interface to control stem-cell fate,” *Nat. Mater.*, vol. 9, no. 6, pp. 518–526, 2010.

[76] C. Branco da Cunha *et al.*, “Influence of the stiffness of three-dimensional alginate/collagen-I interpenetrating networks on fibroblast biology,” *Biomaterials*, vol. 35, no. 32, pp. 8927–8936, 2014.

[77] J. H. Hamman, “Chitosan based polyelectrolyte complexes as potential carrier materials in drug delivery systems,” *Marine Drugs*, vol. 8, no. 4. pp. 1305–1322, 2010.

[78] H. V. Sæther, H. K. Holme, G. Maurstad, O. Smidsrød, and B. T. Stokke, “Polyelectrolyte complex formation using alginate and chitosan,” *Carbohydr. Polym.*, vol. 74, no. 4, pp. 813–821, 2008.

[79] S. J. Florczyk, D. J. Kim, D. L. Wood, and M. Zhang, “Influence of processing parameters on pore structure of 3D porous chitosan-alginate polyelectrolyte complex scaffolds,” *J. Biomed. Mater. Res. - Part A*, vol. 98 A, no. 4, pp. 614–620, 2011.

[80] Z. Li and M. Zhang, “Chitosan-alginate as scaffolding material for cartilage tissue

engineering," *J. Biomed. Mater. Res. - Part A*, vol. 75, no. 2, pp. 485–493, 2005.

[81] Z. Li, M. Leung, R. Hopper, R. Ellenbogen, and M. Zhang, "Feeder-free self-renewal of human embryonic stem cells in 3D porous natural polymer scaffolds," *Biomaterials*, vol. 31, no. 3, pp. 404–412, 2010.

[82] ASTM, "ASTM E112-13: Standard test methods for determining average grain size," *ASTM Int.*, pp. 1–28, 2013.

[83] Z. Pan and J. Ding, "Poly(lactide-co-glycolide) porous scaffolds for tissue engineering and regenerative medicine.," *Interface Focus*, vol. 2, no. 3, pp. 366–77, 2012.

[84] Y.-K. Wang and C. S. Chen, "Cell adhesion and mechanical stimulation in the regulation of mesenchymal stem cell differentiation," *J. Cell. Mol. Med.*, vol. 17, no. 7, pp. 823–832, 2013.

[85] G. S. Huang, L. G. Dai, B. L. Yen, and S. hui Hsu, "Spheroid formation of mesenchymal stem cells on chitosan and chitosan-hyaluronan membranes," *Biomaterials*, vol. 32, no. 29, pp. 6929–6945, 2011.